

A BHLS model based moment analysis of muon $g - 2$, and its use for lattice QCD evaluations of a_μ^{had} .

M. Benayoun^a, P. David^{a,b}, L. DelBuono^a, F. Jegerlehner^{c,d}

^a LPNHE des Universités Paris VI et Paris VII, IN2P3/CNRS, F–75252 Paris, France

^b LIED, Université Paris-Diderot/CNRS UMR 8236, F–75013 PARIS, France

^c Humboldt–Universität zu Berlin, Institut für Physik, Newtonstrasse 15, D–12489 Berlin, Germany

^d Deutsches Elektronen–Synchrotron (DESY), Platanenallee 6, D–15738 Zeuthen, Germany

November 27, 2024

Abstract

We present an up-to-date analysis of muon $g - 2$ evaluations in terms of Mellin-Barnes moments as they might be useful for lattice QCD calculations of a_μ . The moments up to 4th order are evaluated directly in terms of e^+e^- -annihilation data and improved within the Hidden Local Symmetry (HLS) Model, supplied with appropriate symmetry breaking mechanisms. The model provides a reliable Effective Lagrangian (BHLS) estimate of the two-body channels plus the $\pi\pi\pi$ channel up to 1.05 GeV, just including the ϕ resonance. The HLS piece accounts for 80% of the contribution to a_μ . The missing pieces are evaluated in the standard way directly in terms of the data. We find that the moment expansion converges well in terms of a few moments. The two types of moments which show up in the Mellin-Barnes representation are calculated in terms of hadronic cross-section data in the timelike region and in terms of the hadronic vacuum polarization (HVP) function in the spacelike region which is accessible to lattice QCD (LQCD). In the Euclidean the first type of moments are the usual Taylor coefficients of the HVP and we show that the second type of moments may be obtained as integrals over the appropriately Taylor truncated HVP function. Specific results for the isovector part of a_μ^{had} are determined by means of HLS model predictions in close relation to τ -decay spectra.

1 Introduction to the moments expansion approach

In the lattice QCD (LQCD) approach of calculating a_μ^{had} , extrapolation methods have been developed (see e.g. contributions to [1]) to overcome difficulties to reach the physical point in the space of extrapolations. The low Q^2 behavior of the Euclidean electromagnetic current correlators on a lattice, which exhibits a discrete momentum spectrum, poses a particular challenge (see e.g. [2, 3] and references below). Actually, $Q^2 = 0$ is not directly accessible, because of the finite volume, which represents an infrared (IR) cutoff. The analysis of moments of the subtracted (i.e. renormalized) photon vacuum polarization function $\Pi(Q^2) = e^2 \hat{\Pi}(Q^2)$ (e the positron charge) was particularly advocated in variants in Refs. [4] and [5]. Recent lattice calculations [6, 7, 8, 9, 10] have been utilizing moment analysis techniques for a more precise evaluation of a_μ^{had} . The leading moment is given by the slope of the Adler function [11] as follows from the representation:

$$a_\mu^{\text{had}} = \frac{\alpha^2 m_\mu^2}{6\pi^2} \int_0^1 dx x (2-x) (D(Q^2(x))/Q^2(x)) \quad (1)$$

with $Q^2(x) \equiv \frac{x^2}{1-x} m_\mu^2$ the spacelike square momentum transfer, and $D(Q^2)$ the Adler function, defined as a derivative of the shift of the fine structure constant $\Delta\alpha_{\text{had}}(s) \equiv -4\pi\alpha \hat{\Pi}(s)$:

$$D(-s) = -(12\pi^2) s \frac{d\hat{\Pi}(s)}{ds} = \frac{3\pi}{\alpha} s \frac{d}{ds} \Delta\alpha_{\text{had}}(s) . \quad (2)$$

The Adler function is represented by¹:

$$D(Q^2) = Q^2 \left(\int_{4m_\pi^2}^\infty \frac{R(s)}{(s+Q^2)^2} ds \right) \quad (3)$$

in terms of $R(s)$, which can be evaluated in terms of experimental e^+e^- data as well as, to a large part, in terms of our HLS model prediction. The Adler-function $D(Q^2)$ is bounded asymptotically by perturbative QCD (pQCD): $D(Q^2) \rightarrow N_c \sum_f Q_f^2$, with Q_f the quark charges and $N_c = 3$ the color factor, up to perturbative corrections, which asymptotically vanish because of asymptotic freedom which implies $\alpha_s(Q^2) \rightarrow 0$ as $Q^2 \rightarrow \infty$ (see [12]). Obviously, then $D(Q^2)/Q^2$ is a positive monotonically decreasing function bounded by:

$$\frac{D(Q^2)}{Q^2} = \int_{4m_\pi^2}^\infty \frac{R(s)}{(s+Q^2)^2} ds < D'(0) \equiv \int_{4m_\pi^2}^\infty \frac{R(s)}{s^2} ds = \left. \frac{D(Q^2)}{Q^2} \right|_{Q^2=0} , \quad (4)$$

¹We somewhat sloppy write $s_0 = 4m_\pi^2$ for the lower integration limit, which is the threshold for the dominating $\pi^+\pi^-$ channel. However, the true threshold for contributions to $R(s)$ is $s_0 = m_{\pi^0}^2$ as $e^+e^- \rightarrow \pi^0\gamma$ is the process exhibiting the lowest threshold. Most lattice QCD simulations for simplicity are done for the isovector piece, where $4m_\pi^2$ is the correct threshold.

the slope of the vacuum polarization function at zero momentum square. The finite slope guarantees the convergence of the integral (1) at the lower limit. For our analysis it is important to know how the integrand of (1) looks like, in order to know where the important contributions show up. Figure 1 shows a pronounced peak at a surprisingly low scale of about $Q \approx 150$ MeV.

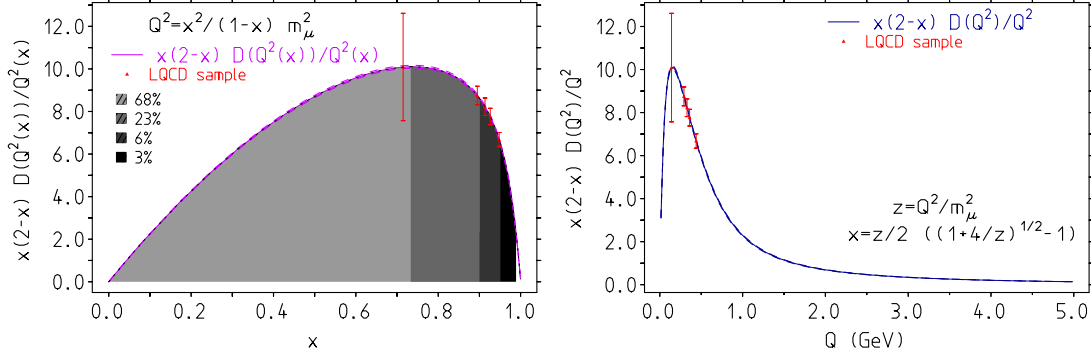


Figure 1: The integrand of the Adler function representation (1) as a function of x and as a function of the energy scale Q . The right-hand panel shows that the integrand is sharply peaked as a function of Q at a rather low scale (~ 150 MeV). Adler function data come from [13]. The dashed lines mark the error band from the experimental data. “LQCD sample” shows points of Q_{\min} from Ref. [14] presently achievable in lattice QCD simulations (shown are pseudo-data lying on the curve, we assumed a 25% uncertainty for the lowest point and a 5% uncertainty for the higher ones). In the left panel we also display the contributions to a_μ^{had} from regions between $Q_i = 0.00, 0.15, 0.30, 0.45$ and 1.0 GeV in percent. The tail above 1 GeV contributes slightly less than 0.2%.

This shows that the dominant ρ contribution appears to be shifted towards lower scales in the Euclidean region.

For the slope, using (2), we may write:

$$D'(0) = -\frac{3\pi}{\alpha} \frac{d}{ds} \Delta\alpha_{\text{had}}(s)|_{s=-Q^2, Q^2 \rightarrow 0} = 12\pi^2 \frac{d}{ds} \hat{\Pi}(s)|_{s=-Q^2, Q^2 \rightarrow 0} \quad (5)$$

directly as the slope of the photon self-energy function $\Pi(Q^2) \equiv 4\pi\alpha\hat{\Pi}(s)$. An evaluation in terms of data yields

$$D'(0) \simeq 10.20(7) \text{ GeV}^{-2} . \quad (6)$$

The Adler function slope $D'(0)$ has been estimated in lattice QCD in [15]. The LQCD result $D'(0) = 5.8(5) \text{ GeV}^{-2}$ has been compared with $D'(0) = 9.81(30) \text{ GeV}^{-2}$, a result obtained using a phenomenological toy-model representation [16] of the isovector spectral function. As another example we mention the result $D'(0) = 12\pi^2 \sum_{u,d,s,c} Q_f^2 \times \Pi_1 = 10.67(17)[9.95(17)] \text{ GeV}^{-2}$

we get with $\Pi_1 = 0.0811(12)[0.0756(13)]$ obtained in Ref. [17] for set 8[10] of Table II, the closest to the physical point. The lattice results usually include the isovector part only, which is simpler but difficult enough, and are often missing some higher energy contributions above 1 GeV.

Note that (1) is equivalent to the standard formula:

$$a_\mu^{\text{had}} = \left(\frac{\alpha m_\mu}{3\pi}\right)^2 \int_{s_0}^{\infty} \frac{ds}{s^2} \hat{K}(s) R(s) \quad (7)$$

in which $\hat{K}(s)$ is a bounded monotonically increasing function, with $\hat{K}(4m_\pi^2) \simeq 0.63$ going to 1 as $s \rightarrow \infty$. Setting $\hat{K}(s) = 1$ we obtain a true upper bound (see also [11]):

$$a_\mu^{\text{had}} < \left(\frac{\alpha m_\mu}{3\pi}\right)^2 D'(0) < 784(6) \times 10^{-10} . \quad (8)$$

The result is way too large as the dominant low energy part of $R(s)$ is obviously overweighted. A lower bound is obtained by setting $\hat{K}(s) = \hat{K}(4m_\pi^2) \approx 0.63$, which implies $a_\mu^{\text{had}} > 494(4) \times 10^{-10}$, again a very rough bound only, but a true bound. These bounds can be much improved by a systematic low energy expansion of the kernel function in (1)², as advocated recently in Ref. [18], specifically as a tool to get more precise results from the Euclidean lattice data. It provides a novel approach for evaluating a_μ^{had} in terms of moments, which goes beyond a simple Taylor expansion of $\Pi(Q^2)$, where the latter, as such, can be integrated only in the range of validity of the expansion. The starting point here is the Mellin-Barnes representation:

$$a_\mu^{\text{had}} = \left(\frac{\alpha}{\pi}\right) \frac{1}{2\pi i} \int_{c-i\infty}^{c+i\infty} ds \mathcal{F}(s) \mathcal{M}(s) \quad (9)$$

with the exact analytic kernel

$$\mathcal{F}(s) = -\Gamma(3-2s) \Gamma(-3+s) \Gamma(1+s), \quad (10)$$

in terms of Euler Gamma functions $\Gamma(s)$. The function $\mathcal{M}(s)$ is the Mellin transform of the hadronic spectral function:

$$\mathcal{M}(s) = \frac{\alpha}{3\pi} \int_{4m_\pi^2}^{\infty} \frac{dt}{t} R(t) \left(\frac{m_\mu^2}{t}\right)^{1-s}, \quad (11)$$

²A low energy expansion of the kernel of (7) is by far not straightforward as we have to deal with the $2m_\mu$ threshold of $\hat{K}(s)$.

and allows to perform a moment expansion by weighting $R(t)$ with powers of m_μ^2/t , as it appears in (11). Remember that $\Gamma(s)$ is a meromorphic function of s with simple poles at $s = -n$ ($n = 0, 1, 2, \dots$) and residues $(-1)^n/n!$. $\Gamma(x)$ is real positive for real positive values of x . The pole structure, which resides on the closed negative real axis, then follows from repeated applications of $\Gamma(s) = \Gamma(s+1)/s$, until $s+1$ is positive.

The low momentum expansion proposed in [18] is derived by calculating the residues of the poles of the above representation (9): $\mathcal{F}(s)$ exhibits simple poles at $s = 0, -1, -2, \dots$ and double poles at $s = -1, -2, \dots$:

$$\begin{aligned} \mathcal{F}(s) \simeq & \frac{1}{3} \frac{1}{s} - \frac{1}{(s+1)^2} + \frac{25}{12} \frac{1}{s+1} - \frac{6}{(s+2)^2} + \frac{97}{10} \frac{1}{s+2} \\ & - \frac{28}{(s+3)^2} + \frac{208}{5} \frac{1}{s+3} - \frac{120}{(s+4)^2} + \frac{3608}{21} \frac{1}{s+4} + \dots \end{aligned} \quad (12)$$

The simple poles yield values:

$$\mathcal{M}(-n) = \frac{\alpha}{3\pi} \int_{4m_\pi^2}^{\infty} \frac{ds}{s} R(s) \left(\frac{m_\mu^2}{s} \right)^{1+n}. \quad (13)$$

The double poles of $\mathcal{F}(s)$ also require the first derivative of the Mellin transform:

$$\tilde{\mathcal{M}}(-n) = \frac{\alpha}{3\pi} \int_{4m_\pi^2}^{\infty} \frac{ds}{s} R(s) \ln\left(\frac{m_\mu^2}{s}\right) \left(\frac{m_\mu^2}{s}\right)^{1+n} = -\frac{d}{ds} \mathcal{M}(s)|_{s=-n}. \quad (14)$$

In terms of the moments, the successive approximations then read:

$$\begin{aligned} a_\mu^{\text{had}}(0) &= \left(\frac{\alpha}{\pi}\right) \left[\frac{1}{3} \mathcal{M}(0)\right] \\ a_\mu^{\text{had}}(1) &= a_\mu^{\text{had}}(0) + \left(\frac{\alpha}{\pi}\right) \left[\frac{25}{12} \mathcal{M}(-1) + \tilde{\mathcal{M}}(-1)\right] \\ a_\mu^{\text{had}}(2) &= a_\mu^{\text{had}}(1) + \left(\frac{\alpha}{\pi}\right) \left[\frac{97}{10} \mathcal{M}(-2) + 6\tilde{\mathcal{M}}(-2)\right] \\ a_\mu^{\text{had}}(3) &= a_\mu^{\text{had}}(2) + \left(\frac{\alpha}{\pi}\right) \left[\frac{208}{5} \mathcal{M}(-3) + 28\tilde{\mathcal{M}}(-3)\right] \\ a_\mu^{\text{had}}(4) &= a_\mu^{\text{had}}(3) + \left(\frac{\alpha}{\pi}\right) \left[\frac{3608}{21} \mathcal{M}(-4) + 120\tilde{\mathcal{M}}(-4)\right], \end{aligned} \quad (15)$$

Note that $\mathcal{M}(0)$ corresponds to the Adler function slope $D'(0)$ in (8) as $\mathcal{M}(0) = \frac{\alpha}{3\pi} m_\mu^2 D'(0)$.

The analysis presented in the following includes e^+e^- annihilation data from Novosibirsk (NSK) [19, 20, 21], Frascati (KLOE) [22, 23, 24], Stanford (BaBar) [25] and Beijing (BES-III) [26], τ -decay data from ALEPH, OPAL, CLEO and Belle [27, 28, 29, 30, 31]. Other

data on exclusive channels recently collected, and published up to the end of 2014, include the $e^+e^- \rightarrow 3(\pi^+\pi^-)$ data from CMD-3 [32], the $e^+e^- \rightarrow \omega\pi^0 \rightarrow \pi^0\pi^0\gamma$ from SND [33] and several data sets collected by BaBar in the ISR mode³ [34, 35, 36, 37].

In the following we present results for the moments directly in terms of e^+e^- annihilation data as well as global fit improved BHLS estimates for moments up to the 4th order, which allow us to get good estimates for the full results. The main results, the evaluations of the moments $\mathcal{M}(-n)$ and $\tilde{\mathcal{M}}(-n)$ for $n = 0, 1, 2, 3, 4$ and the corresponding results for $a_\mu^{\text{had}}(n)$, are presented in Sect. 2. While the moments $\mathcal{M}(-n)$ are directly calculable by the Euclidean methods of lattice QCD, the moments $\tilde{\mathcal{M}}(-n)$ are only indirectly accessible in the Euclidean world. Therefore, in Sect. 3 we perform a related calculation in terms of other types of moments, denoted by $\Sigma(-n; s_0)$, which are directly accessible to lattice QCD calculations and allow one to estimate $\tilde{\mathcal{M}}(-n)$ as linear combinations of $\Sigma(-n; s_0)$'s and of higher order $\mathcal{M}(-n)$'s. As indicated, the auxiliary moments $\Sigma(-n; s_0)$'s depend on an infrared cutoff s_0 which should cancel in the linear combination which corresponds to $\tilde{\mathcal{M}}(-n)$, which by definition is independent of s_0 . In Sect. 4 we have a closer look on the method studied in Sect. 3, which follows the line proposed in Ref. [18]. A more careful consideration reveals that also the log suppressed moments $\tilde{\mathcal{M}}(-n)$ can be obtained directly from Euclidean momentum space by a limiting procedure $s_0 \rightarrow 0$ of an integral over a truncated HVP function. Sect. 5 is devoted to the extraction of the I=1 part of the HVP function and its contribution to the various moments. It also provides more details concerning the role of τ -decay spectral data and the isospin breaking effects in the HLS model. Isospin breaking effects, and particularly vector meson mixing effects together and with the photon, have to be included in order to properly relate the isovector τ data to e^+e^- annihilation data. This provides insight into the model dependence of the BHLS evaluations. Conclusions are presented in Sect. 6. For recent summaries of a_μ^{had} evaluations we refer to [38, 39, 40].

2 A BHLS model based moment analysis of a_μ^{had}

Previous studies [41, 42] have shown that the Hidden Local Symmetry (HLS) Model, supplied with appropriate symmetry breaking mechanisms, provides an Effective Lagrangian (BHLS) which encompasses a large number of processes within a unified framework. A global fit procedure has been derived herefrom which allows for a simultaneous description of the e^+e^- annihilation into 6 final states – $\pi^+\pi^-$, $\pi^0\gamma$, $\eta\gamma$, $\pi^+\pi^-\pi^0$, K^+K^- , K_LK_S – and includes the dipion spectrum in the τ decay and some more light meson decay partial widths. The contribution to the muon anomalous magnetic moment a_μ^{th} of these annihilation channels over the

³Including the $p\bar{p}$, K^+K^- , K_LK_S , $K_LK_S\pi^+\pi^-$, $K_SK_S\pi^+\pi^-$, $K_SK_SK^+K^-$ final states.

range of validity of the HLS model (up to 1.05 GeV) is found much improved compared to the standard approach of integrating the measured e^+e^- spectra directly [41, 42]. The key point is that besides implementing the vector meson dominance model (VDM) in accord with the chiral structure of QCD, the model allows to treat the mixing of ρ , ω , and ϕ among them and with the *photon* in a coherent way as a consequence of the vector meson self-energy effects, which at the same time models the vector meson widths and the related decays, and in particular models the relationship between e^+e^- annihilations and the charged τ channel. In contrast to the standard approach of integrating the e^+e^- data, the BHLS approach incorporates the τ spectral data as a key ingredient. This provides a welcome reduction of the leading hadronic uncertainty in the lowest order (LO) hadronic vacuum polarization (HVP) to a_μ . Here we apply our approach to the moments analysis of a_μ^{had} .

Table 1: Moments of the a_μ^{had} -expansion in units 10^{-5} . Here $\mathcal{M}(-n)$ and $\tilde{\mathcal{M}}(-n)$ are evaluated via Eqs. (13) and (14) in terms of $R(s)$ as provided by e^+e^- annihilation data and/or predictions of the BHLS model Lagrangian. The “data HLS channels” denote the channels separated from the $R(s)$ “data direct”, which are predicted by means of the HLS effective Lagrangian after determining its parameters by a global fit. The prediction “HLS model” is then combined with the remainder represented by the difference of the first two columns in column 4 as “HLS + remainder”. Note the remarkable gain in accuracy when replacing the “data HLS channels” by the “HLS model” prediction. The improvement gets the better the higher the moment is, since higher moments are more and more dominated by the low energy tail covered by the HLS model.

moment	data direct		data HLS channels		HLS model		HLS + remainder	
$\mathcal{M}(0)$	10.1307	± 0.0745	8.6275	± 0.0495	8.6041	± 0.0130	10.1073	± 0.0572
$\mathcal{M}(-1)$	0.23507	± 0.00185	0.22944	± 0.00184	0.23197	± 0.00031	0.23760	± 0.00038
$\mathcal{M}(-2)$	0.008702	± 0.000115	0.008669	± 0.000115	0.008974	± 0.000011	0.009007	± 0.000011
$\mathcal{M}(-3)$	0.0004852	± 0.0000093	0.0004850	± 0.0000093	0.0005147	± 0.0000064	0.0005149	± 0.0000064
$\mathcal{M}(-4)$	0.00003676	± 0.0000083	0.00003676	± 0.0000083	0.00003956	± 0.0000005	0.00003956	± 0.0000005
$\tilde{\mathcal{M}}(-1)$	-0.82592	± 0.00516	-0.79611	± 0.00501	-0.80054	± 0.00113	-0.83035	± 0.00168
$\tilde{\mathcal{M}}(-2)$	-0.026808	± 0.000294	-0.026644	± 0.000294	-0.027338	± 0.000035	-0.027503	± 0.000035
$\tilde{\mathcal{M}}(-3)$	-0.0013160	± 0.0000228	-0.0013149	± 0.0000228	-0.0013847	± 0.0000017	-0.0013858	± 0.0000017
$\tilde{\mathcal{M}}(-4)$	-0.00009064	± 0.00000199	-0.00009063	± 0.00000199	-0.00009725	± 0.00000012	-0.00009726	± 0.00000012

An up-to-date evaluation of the moments, based on a $R(s)$ compilation of e^+e^- annihilation data together with the results using the BHLS predictions is presented in Table 1. The improvement obtained by modeling the channels encompassed by the BHLS model is what we observe going from “data HLS channels” to “HLS model”, which then is supplemented by the part not covered

Table 2: The LO-HVP contribution in terms of moments in units 10^{-10}

	data direct	data HLS channels	HLS model	HLS + remainder
$a_\mu^{\text{had}}(0)$	784.39 ± 5.77	668.00 ± 3.83	666.19 ± 1.01	782.58 ± 4.43
$a_\mu^{\text{had}}(1)$	706.30 ± 5.47	594.11 ± 3.56	592.50 ± 0.89	704.69 ± 4.21
$a_\mu^{\text{had}}(2)$	688.55 ± 5.31	576.51 ± 3.41	574.62 ± 0.87	686.65 ± 4.19
$a_\mu^{\text{had}}(3)$	684.68 ± 5.26	572.65 ± 3.35	570.58 ± 0.87	682.61 ± 4.19
$a_\mu^{\text{had}}(4)$	683.62 ± 5.23	571.59 ± 3.33	569.45 ± 0.86	681.48 ± 4.18
a_μ^{had}	683.50 ± 4.75	570.68 ± 3.67	568.95 ± 0.89	681.77 ± 3.14

by the effective Lagrangian in its range of validity to obtain the best evaluation for ‘‘HLS + remainder’’. The evaluation of a_μ^{had} in terms of these moments follows in Table 2. The bottom entries are the results obtained with the exact kernel, as presented in the previous section. The errors of the moments are 100% correlated although weighted differently for different energy regions. Since the signed errors are added linearly with weight unity, errors apparently get somewhat underestimated⁴. One observes a nice convergence provided all contributions are collected appropriately. One should keep in mind that the dominating ρ resonance accounts for about 75% and the predictable HLS channels account for about 80% of a_μ^{had} . Thus, obviously, the non-HLS contribution including data at higher energies (beyond our 1.05 GeV breakpoint) is important in getting the complete results. Figure 2 illustrates the fast convergence of the first few moments, despite the fact that the lowest order moment is quite far off. Therefore, in cases where the relevant moments are available rather than $R(s)$, e.g. in lattice QCD, the Mellin-Barnes moments approach, suggested in Ref. [18], provides a reliable method for the evaluation of a_μ^{had} .

It is worthwhile to add a comment about the HLS model estimates of the moments. While the direct data evaluation is based simply on weighted averages of data sets which then are integrated using the trapezoidal rule, the HLS model results are obtained by the Monte Carlo method. The BHLS global fit using `Minuit` provides: i/ the vector \vec{x} of the central values of the fit parameters ii/ the error covariance matrix V . These are treated as the parameters of a multidimensional Gaussian distribution $G(x, V)$, of which one performs N (a few hundreds or thousands) samplings. For each sampling one calculates the function $R(s)$. So, we have numerically N estimates of the function $R(s)$: $R(s, i)$, $i = 1, \dots, N$ all defined in steps of

⁴Adding errors quadratically would be simply wrong here. a_μ^{had} is dominated by the $\pi^+\pi^-$ channel and there by the systematic error. The dominance of the $\pi^+\pi^-$ channel gets even more pronounced the higher the moment. As all moments are linear in $R(s)$, if R goes up the $\mathcal{M}(-n)$ ’s go up and all $\tilde{\mathcal{M}}(-n)$ ’s go down. The different weighting for different n does not make them independent. Rather the \mathcal{M} ’s are close to 100% correlated while the $\tilde{\mathcal{M}}$ ’s are 100% anti-correlated relative to the \mathcal{M} ’s. Our error estimate is to be considered as an educated guess.

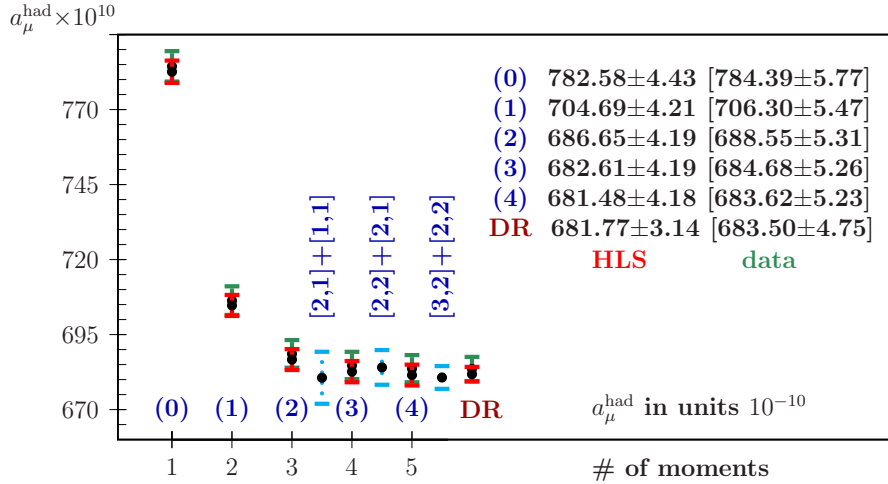


Figure 2: Starting with a crudely overestimated approximation, the successive higher moments converge rapidly. Shown are results from Table 2 for “data direct” and “HLS + remainder”. DR marks the result obtained with the dispersion relation (7). Shown are also the Taylor-Padé estimates of Table 3 based on 3, 4 and 5 Taylor coefficients.

0.5 MeV from threshold to 1.05 GeV. One then can estimate any moment

$$Q = \int K_Q(s) R(s) ds ,$$

with the appropriate kernel $K_Q(s)$, to obtain sequences

$$Q(i) = \int K_Q(s) R(s, i) ds, i = 1 \dots N .$$

Then, the $Q(i)$ sequence can be histogrammed and fitted by a Gaussian from which one derives the central value and the standard deviation (this is done easily within `PAW`).

For what concerns the data direct approach, we use chiral perturbation theory to parametrize a fit of the low energy tail of the available data (including timelike as well as spacelike data up to 400 MeV) [43]. Integrals are then performed adopting 318 MeV as a “chiral cut”, below which the fit is used in place of the data compilation. Since the higher moments are completely dominated by the HLS channels and the high energy tail above 1.05 GeV also gets negligible, the higher moments directly reflect the difference of the HLS model versus the standard data direct approach.

3 Moments accessible in lattice QCD calculations

In this section we study the Mellin-Barnes moment (MBM) approach in terms of Euclidean quantities as proposed in [18]. The phenomenologically estimated moments provide useful tests for lattice results since the moments

$$\mathcal{M}(-n) = \frac{(-1)^{(n+1)}}{(n+1)!} (m_\mu^2)^{n+1} \left(\frac{\partial^{n+1}}{(\partial Q^2)^{n+1}} \Pi(Q^2) \right) \Big|_{Q^2=0}. \quad (16)$$

are directly accessible by lattice QCD. A comparison with the Taylor expansion

$$\Pi(Q^2) = \sum_{n=0}^{\infty} (Q^2)^{(n+1)} \frac{1}{(n+1)!} \left(\frac{\partial^{n+1}}{(\partial Q^2)^{n+1}} \Pi(Q^2) \right) \Big|_{Q^2=0} = \sum_{n=0}^{\infty} (Q^2)^{(n+1)} \Pi_{n+1}, \quad (17)$$

reveals that the moments $\mathcal{M}(-n)$, up to normalization, agree with the normal Taylor coefficients of the low energy expansion of $\Pi(Q^2)$:

$$\Pi_{n+1} = (-1)^{(n+1)} (m_\mu^2)^{-(n+1)} \mathcal{M}(-n). \quad (18)$$

Up to a factor $4\pi\alpha Q_f^2$ summed over the $n_f = 4$ flavors f included, these are the moments used in the recent analysis [17], for example⁵. A partial integration allows us to rewrite (1) directly as an integral over the vacuum polarization amplitude [44, 45]

$$a_\mu^{\text{had}} = \frac{\alpha}{\pi} \int_0^1 dx (1-x) \Delta\alpha_{\text{had}}(-Q^2(x)) = -\frac{\alpha}{\pi} \int_0^1 dx (1-x) \Pi(Q^2(x)) \quad (19)$$

and inserting the Taylor expansion for $\Pi(Q^2(x))$, with $Q^2(x) \equiv \frac{x^2}{1-x} m_\mu^2$ we get

$$a_\mu^{\text{had}} = \frac{\alpha}{\pi} \sum_{n=0}^{\infty} (-1)^n \mathcal{M}(-n) \int_0^{x_1} dx x^2 \left(\frac{x^2}{1-x} \right)^n - \frac{\alpha}{\pi} \int_{x_1}^1 dx (1-x) \Pi(Q^2(x)), \quad (20)$$

⁵The uncorrected Taylor coefficients for sets 8 and 10 (the closest to the physical point) of Table II in [17] translate into $\mathcal{M}(-n) = 4\pi\alpha \sum Q_f^2 (-1)^n (m_\mu^2)^{n+1} \Pi_{n+1}$ as follows:

Π_1	=	0.0811(12)	Π_2	=	0.1238(36)	Π_3	=	0.205(9)	Π_4	=	0.344(20)
$\mathcal{M}(0)$	=	9.23(14)	$\mathcal{M}(-1)$	=	0.1572(46)	$\mathcal{M}(-2)$	=	0.00291(13)	$\mathcal{M}(-3)$	=	0.000054(3)
Π_1	=	0.0756(13)	Π_2	=	0.1111(41)	Π_3	=	0.179(11)	Π_4	=	0.293(25)
$\mathcal{M}(0)$	=	8.60(15)	$\mathcal{M}(-1)$	=	0.1411(52)	$\mathcal{M}(-2)$	=	0.00254(16)	$\mathcal{M}(-3)$	=	0.000046(4)

to be compared with the HLS model column of Table 1. Note that substantial corrections to be applied to the raw data are not included here.

which requires an appropriate energy cutoff $x_1 < 1$ at which the low momentum expansion ceases to make sense. Obviously, the expansion collapses for an upper limit $x_1 = 1$. Not surprisingly, the problem is the high energy tail; an Euclidean cutoff Q_1^2 indeed provides an effective $x_1 = \frac{q_1^2}{2} \sqrt{1 + 4/q_1^2} - 1 \approx 1 - 1/q_1^2 + \dots$ where $q_1 = Q_1/m_\mu$. Here we are confronted with the question about the dependence of the result on the cutoff. This is different for the timelike representation (7), due to the $1/s^2$ behavior of the kernel, while $R(s)$ approaches a constant. The cutoff dependence is suppressed by $1/E_1^2$ for high enough cutoffs E_1 in this case. In order to learn where the dominant contributions come from, we plot the integrand of (19) in Fig. 3. Also in the Euclidean region the integrand is highly peaked, now around half of the ρ meson mass scale.

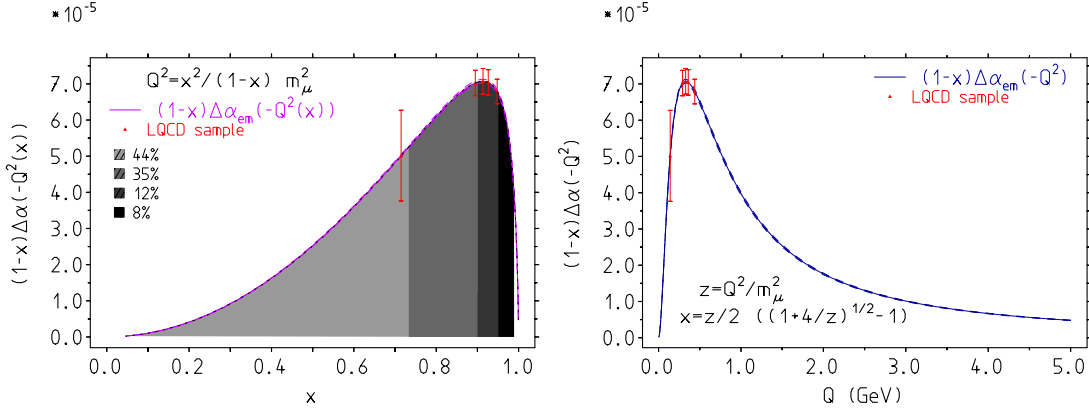


Figure 3: The integrand of the vacuum polarization representation (19) as a function of x and as a function of the energy scale Q . As we see the integrand is strongly peaked as a function of Q at about 330 MeV. $\Pi(Q^2)$ data come from [46]. The dashed lines mark the error band from the experimental data. “LQCD sample” as in Fig. 1. In the left panel we again display the contributions to a_μ^{had} from regions between $Q_i = 0.00, 0.15, 0.30, 0.45$ and 1.0 GeV in percent. The tail above 1 GeV contributes slightly less than 1%. Note the different distribution of the contributions from the different ranges for the Adler function integral representation (see left panel of Fig. 1).

Lattice QCD groups usually use a different representation for the a_μ^{had} dispersion integral:

$$a_\mu^{\text{had}}[Q_{\text{max}}^2] = \frac{\alpha}{\pi} \int_0^{Q_{\text{max}}^2} dQ^2 f(Q^2) (-4\pi\alpha\hat{\Pi}(Q^2)), \quad (21)$$

with

$$f(Q^2) = m_\mu^2 Q^2 Z^3(Q^2) (1 - Q^2 Z(Q^2)) / (1 + m_\mu^2 Q^2 Z^2(Q^2))$$

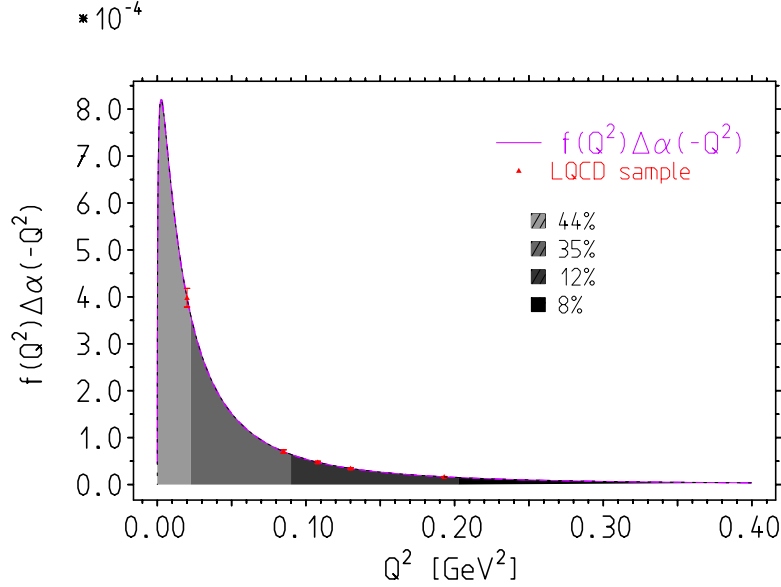


Figure 4: The integrand of (21), which represents (19) as an integral over Q^2 . Ranges between $Q_i = 0.00, 0.15, 0.30, 0.45$ and 1.0 GeV and their percent contribution to a_μ^{had} and the “LQCD sample” as in Fig. 3.

and

$$Z(Q^2) = \left(\sqrt{Q^4 + 4m_\mu^2 Q^2} - Q^2 \right) / (2m_\mu^2 Q^2).$$

In our notation $-4\pi\alpha\hat{\Pi}(Q^2) = \Delta\alpha_{\text{had}}(-Q^2)$. See e.g. Figure 1 of [14] which in our representations (19) and (1) translates into our Figs. 3 and 1, respectively. The contributions to a_μ^{had} from the ranges displayed in the left panel of Fig. 3 are the same. This is illustrated in Fig. 4. We note that in the representation (1), in terms of the Adler function, the contribution obtained for a given Q_{min} is substantially smaller than in the representations (19) or (21), which integrate the HVP function directly.

In the lattice QCD approach, the current correlator defining $\Pi(Q^2)$ is evaluated in configuration space, and one would have to perform a Fourier transformation, which, for obvious reasons, is not so straightforward with the discrete lattice data. The moments Π_n of Eq. (18), on the other hand are directly accessible by calculating

$$G_{2j} \equiv \sum_t \sum_{\vec{x}} t^{2j} Z_V^2 \langle j^i(\vec{x}, t) j^i(0) \rangle = (-1)^j \frac{\partial^{2j}}{\partial k^{2j}} k^2 \hat{\Pi}(k^2) \Big|_{k^2=0} = (-1)^j (2j!) \Pi_{j-1}, \quad (22)$$

where Z_V is the lattice vector current renormalization factor and the sums extend over the time

t and space \vec{x} lattice points. So, what is available primarily is the low momentum expansion only. In order to get a useful $\Pi(Q^2)$ for the higher momenta, one usually calculates the Padé approximants [17], which then allow for an acceptable estimate of the full contribution. In Fig. 5 we show results in comparison with $\Delta\alpha_{\text{had}}$. Best bounds are the Padés of type $[n,n]$ as lower

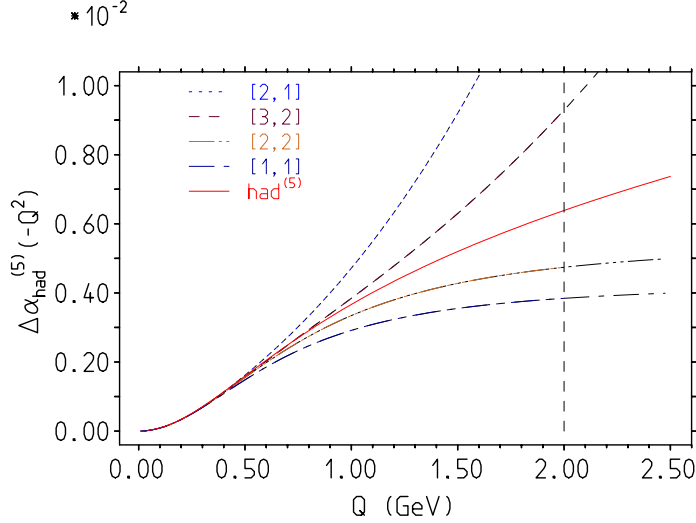


Figure 5: $\Delta\alpha_{\text{had}}$ as a function of the spacelike momentum transfer Q together with the best pairs of Padé approximants ($[1,1]$ and $[2,1]$) and ($[2,2]$ and $[3,2]$), which can be formed given 4 and 5 moments $\mathcal{M}(-n)$ ($n = 0, 1, 2, 3, 4$), respectively. Keep in mind that the reference scale of our moment expansion is the muon mass m_μ and higher momenta get suppressed in the a_μ^{had} integral. The “exact” $\Delta\alpha_{\text{had}}$ labeled by $\text{had}^{(5)}$ comes from [46].

bound accompanied by $[n+1,n]$ as upper constraint, which requires $2n + 1$ coefficients⁶. For the five moments we have worked out, adopting the moments “HLS+remainder”, the best Padé approximants are $[1,1]$ and $[2,1]$ requiring 3 moments, $[2,1]$ and $[2,2]$ requiring 4 moments and $[2,2]$ and $[3,2]$ for given 5 moments. The integrals of the Padés are listed in Table 3 together with the result from the direct integration (DR) and from the MBM expansion of order $n = 4$ (five moments $\mathcal{M}(-n)$ and four moments $\tilde{\mathcal{M}}(-n)$). The upper bound Padés $[2,1]$ and $[3,2]$ are combined with the lower bound ones $[1,1]$ and $[2,2]$, respectively, taking half of the sums and adding half of the difference as a model error in quadrature. The different results are in good agreement with each other. We have used that the factor $(1 - x)$ in (20) acts as a $1/Q^2$ factor

⁶The number of coefficients of a Padé approximant $[m,n]=\sum_{k=0}^m a_k x^k / (1 + \sum_{k=1}^n b_k x^k)$ is $n + m + 1$ unless $a_0 = 0$ as in case of the HVP $\Pi(Q^2)$ or the Adler function $D(Q^2)$, where it is $n + m$. Padés for $D(Q^2)/Q^2$ and for the truncated HVP $\Pi(Q^2)_n^{\text{trunc}}/(Q^2)^{n+1}$ considered in Sect. 4 require $n + m + 1$ coefficients, however.

Table 3: $a_\mu^{\text{had}} \times 10^{10}$ from the Padé approximants of the $\Pi(Q^2)$ Taylor expansion in Q^2/m_μ^2 , given 3, 4 and 5 coefficients of the “HLS + remainder” moments.

3 Taylor coefficients			4 Taylor coefficients			5 Taylor coefficients		
[1,1]	672.21 ± 4.16		[2,1]	688.96 ± 4.24		[2,2]	679.13 ± 4.20	
[2,1]	688.96 ± 4.24		[2,2]	679.13 ± 4.20		[3,2]	682.23 ± 4.22	
[1,1]+[2,1]	680.58 ± 9.37		[2,1]+[2,2]	684.04 ± 6.48		[2,2]+[3,2]	680.68 ± 4.49	
DR			681.77 ± 3.14	MBM		681.48 ± 4.18		

at high energy, such that the $[n+1,n]$ Padés are not in conflict with integrability. Nevertheless, the Padés cannot be arranged to be in accord with QCD asymptotics and a suitable modification taking into account this fact is appropriate. In the Euclidean region the “experimental” Adler function can be used to check the validity of pQCD [12]. One finds that pQCD works pretty accurately above about 2 GeV to 2.5 GeV. We have adopted a cutoff of $Q_1 = 2$ GeV in order to obtain the results in Fig. 5 and Table 3, where we use $\Delta\alpha_{\text{had}}(-Q^2)$ for momenta $Q > Q_1$. In fact the results presented do not substantially depend on the cut and remain within uncertainties.

Similarly, we may look at the “Taylor + Padé” method for the Adler function representation (1). From (17) and (18), we learn that, given the HVP function Taylor coefficients

$$\Pi(Q^2) = \sum_{n=0}^{\infty} (Q^2)^{(n+1)} (-1)^{(n+1)} (m_\mu^2)^{-(n+1)} \mathcal{M}(-n), \quad (23)$$

the corresponding Adler function ones follow by the replacement $\mathcal{M}(-n) \rightarrow (n+1) \mathcal{M}(-n)$ as

$$D(Q^2) \propto -Q^2 \frac{d}{dQ^2} \Pi(Q^2) = \sum_{n=0}^{\infty} (Q^2)^{(n+1)} (-1)^n (m_\mu^2)^{-(n+1)} (n+1) \mathcal{M}(-n). \quad (24)$$

Equations (1) and (2) suggest to consider

$$\hat{\mathcal{D}}(Q^2) \equiv \frac{\alpha}{3\pi} m_\mu^2 D(Q^2)/Q^2 \quad (25)$$

and expand in Q^2/m_μ^2 . The corresponding best Padés are shown in Fig. 6, where “best” cases are chosen such that they match best the “experimental” curve, extracted by means of (3) from e^+e^- data, towards higher energies. Note that the Padés for $\hat{\mathcal{D}}(Q^2)$ differ from those of the HVP function as, by definition, its Taylor expansion starts with a constant term. Given 5 coefficients, the best estimate is given in Table 4 by the pair [1,2] and [1,3].

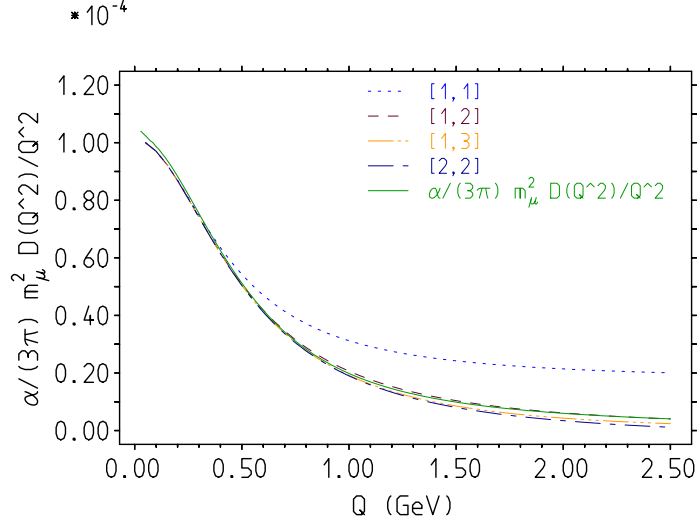


Figure 6: Comparison of the best Padé approximants for the Taylor expansion of $\frac{\alpha}{3\pi} m_\mu^2 D(Q^2)/Q^2$, which enters the representation (1). The best pair of Padés for our set of 5 coefficients are [1,2] as upper and [1,3] (or [2,2]) as lower bound. Most of the Padés fail to represent the data towards higher energies. The “exact” Adler function ratio $D(Q^2)/Q^2$ comes from [13].

Table 4: $a_\mu^{\text{had}} \times 10^{10}$ from the Padé approximants of the Taylor expansion of $D(Q^2)/Q^2$, given 5 coefficients of the “HLS + remainder” moments.

[1,2]	681.35 ± 4.21	[1,3]	680.74 ± 4.25	[1,2]+[1,3]	681.05 ± 4.24
-------	-------------------	-------	-------------------	-------------	-------------------

In contrast to the Taylor expansion approach, the Mellin-Barnes representation provides a convergent expansion in terms of the moments $\mathcal{M}(-n)$ and $\tilde{\mathcal{M}}(-n)$. The log weighted moments $\tilde{\mathcal{M}}(-n)$ are related to properties of $\Pi(Q^2)$ in a more complicated manner [18] and require, in addition, to determine the moments

$$\Sigma(-n; Q_0^2) \equiv \int_{Q_0^2}^{\infty} dQ^2 \left(\frac{m_\mu^2}{Q^2} \right)^{n+1} \left(-\frac{\Pi(Q^2)}{Q^2} \right) \quad (26)$$

for $n = 1, 2, 3, \dots$. Note that there is here an ambiguity in the choice of Q_0^2 as these are not integrals along a cut, as the integrals over $R(s)$ are. Nevertheless, we need $Q_0^2 > 0$ to provide an infrared cutoff, in order for the low momentum expansion moments to exist. As suggested

in [18] we may adopt the choice $Q_0^2 = 4m_\pi^2$. However, $Q_0^2 = m_{\pi^0}^2$ may be a better choice as will seen below, where we compare the two choices

$$Q_0^2 = m_{\pi^0}^2 \quad \text{and} \quad Q_0^2 = 4m_\pi^2. \quad (27)$$

The relation between $\tilde{\mathcal{M}}(-n)$ and $\Sigma(-n; s_0)$, which also involves the moments $\mathcal{M}(-n)$, can be found by means of applying the subtracted dispersion relation:

$$-\frac{\Pi(Q^2)}{Q^2} = \frac{\alpha}{3\pi} \int_{4m_\pi^2}^{\infty} \frac{ds}{s} \frac{R(s)}{s+Q^2}. \quad (28)$$

We note that the Euclidean moments $\Sigma(-n; s_0)$ in terms of $R(s)$ appear represented as double integrals, where the first integration transforms the timelike $R(s)$ information into the spacelike vacuum polarization function $\Pi(Q^2)$, a smoothed object, devoid of thresholds and of resonance peaks. However, interchanging integrations, the first integration represents a kernel $J(s_0, s; n)$ which, for each n , can be performed analytically. Therefore, also in this case, one ends up with a one-dimensional integral representation. For $\Sigma(-n; s_0)$ in terms of moments one obtains:

$$\begin{aligned} \Sigma(-n; s_0) &= \frac{\alpha}{3\pi} \int_{4m_\pi^2}^{\infty} \frac{ds}{s} R(s) J(s_0, s; n) \\ J(s_0, s; n) &= \int_{Q_0^2=s_0}^{\infty} dQ^2 \left(\frac{m_\mu^2}{Q^2} \right)^{n+1} \frac{1}{s+Q^2}. \end{aligned} \quad (29)$$

The second integral can be performed analytically and up to 3rd order yields:

$$\begin{aligned} J(s_0, s; 1) &= -\ln\left(1 + \frac{s}{s_0}\right) \left(\frac{m_\mu^2}{s}\right)^2 + \frac{m_\mu^2}{s_0} \frac{m_\mu^2}{s} \\ J(s_0, s; 2) &= \ln\left(1 + \frac{s}{s_0}\right) \left(\frac{m_\mu^2}{s}\right)^3 - \frac{m_\mu^2}{s_0} \left(\frac{m_\mu^2}{s}\right)^2 + \frac{1}{2} \left(\frac{m_\mu^2}{s_0}\right)^2 \frac{m_\mu^2}{s} \\ J(s_0, s; 3) &= -\ln\left(1 + \frac{s}{s_0}\right) \left(\frac{m_\mu^2}{s}\right)^4 + \frac{m_\mu^2}{s_0} \left(\frac{m_\mu^2}{s}\right)^3 - \frac{1}{2} \left(\frac{m_\mu^2}{s_0}\right)^2 \left(\frac{m_\mu^2}{s}\right)^2 \\ &\quad + \frac{1}{3} \left(\frac{m_\mu^2}{s_0}\right)^3 \frac{m_\mu^2}{s}. \end{aligned} \quad (30)$$

Then, using $\ln(1 + \frac{s}{s_0}) = -\ln(\frac{m_\mu^2}{s}) - \ln(\frac{s_0}{m_\mu^2}) + \ln(1 + \frac{s_0}{s})$, we obtain:

$$\begin{aligned}
\Sigma(-1; s_0) &= \tilde{\mathcal{M}}(-1) + \ln \frac{s_0}{m_\mu^2} \mathcal{M}(-1) + \frac{m_\mu^2}{s_0} \mathcal{M}(0) - \mathcal{R}(-1; s_0) \\
\Sigma(-2; s_0) &= -\tilde{\mathcal{M}}(-2) - \ln \frac{s_0}{m_\mu^2} \mathcal{M}(-2) - \frac{m_\mu^2}{s_0} \mathcal{M}(-1) + \frac{1}{2} \left(\frac{m_\mu^2}{s_0} \right)^2 \mathcal{M}(0) + \mathcal{R}(-2; s_0) \\
\Sigma(-3; s_0) &= \tilde{\mathcal{M}}(-3) + \ln \frac{s_0}{m_\mu^2} \mathcal{M}(-3) + \frac{m_\mu^2}{s_0} \mathcal{M}(-2) - \frac{1}{2} \left(\frac{m_\mu^2}{s_0} \right)^2 \mathcal{M}(-1) \\
&\quad + \frac{1}{3} \left(\frac{m_\mu^2}{s_0} \right)^3 \mathcal{M}(0) - \mathcal{R}(-3; s_0)
\end{aligned} \tag{31}$$

with the ‘‘remainder’’:

$$\mathcal{R}(-n; s_0) = \frac{\alpha}{3\pi} \int_{4m_\pi^2}^{\infty} \frac{ds}{s} R(s) \ln \left(1 + \frac{s_0}{s} \right) \left(\frac{m_\mu^2}{s} \right)^{n+1}. \tag{32}$$

The latter can be evaluated in terms of e^+e^- data and BHLS predictions, but they are not directly accessible by lattice data. However, in this representation the log can be expanded as $\ln(1+x) = \sum_{n=1}^{\infty} (-1)^{n+1} \frac{x^n}{n}$ which converges for $-1 < x \leq 1$ and we obtain a series of normal moments $\mathcal{M}(-n)$ accessible by LQCD. We thus have

$$\mathcal{R}(-n; s_0) \approx \frac{s_0}{m_\mu^2} \mathcal{M}(-n-1) - \frac{1}{2} \left(\frac{s_0}{m_\mu^2} \right)^2 \mathcal{M}(-n-2) + \dots \tag{33}$$

Here we see that the choice of s_0 , or Q_0^2 in (26), respectively, is not uncritical, if we want the series to converge well. For the isovector part $0 < s_0 \leq 4m_\pi^2$ is adequate. For the full electromagnetic case, with m_{π_0} being the true threshold $0 < s_0 \leq m_{\pi_0}^2$ is appropriate. The results are presented in Table 5. While the approximate results $\mathcal{R}^\approx(-n; s_0)$ agree fairly well for $s_0 = m_{\pi_0}^2$ with the direct evaluations $\mathcal{R}^*(-n; s_0)$, for $s_0 = 4m_\pi^2$ the agreement is not convincing. One has to keep in mind that a_μ^{had} evaluations are required with high precision.

Knowing the remainders $\mathcal{R}(-n; s_0)$, either by direct integration of (32) or using their expansion in terms of moments $\mathcal{M}(-n)$ we are able to calculate the Euclidean moments $\Sigma(-n; s_0)$ via $R(s)$ data or BHLS model predictions with the help of the relations (31) in terms of the moments and remainders given in Table 1 and Table 5, respectively. Table 6 lists the results of this evaluation. As mentioned earlier, the moments $\Sigma(-n; s_0)$ are very much dependent on

Table 5: The remainders $\mathcal{R}(-n; s_0)$ in units 10^{-5} for $s_0 = m_{\pi_0}^2$ in the upper part and for $s_0 = 4m_{\pi}^2$ in the lower part. The $\mathcal{R}^*(-n; s_0)$ are evaluated in via (32) the same way as the moments of Table 1. The remainders $\mathcal{R}^\approx(-n; s_0)$ are calculated via the expansion (33) in terms of the moments $\mathcal{M}(-n)$ from Table 1

moment	data direct		data HLS channels		HLS model		HLS + remainder	
$\mathcal{R}^*(-1; m_{\pi_0}^2)$	0.013602	± 0.000177	0.013549	± 0.000177	0.014010	± 0.000018	0.014063	± 0.000020
$\mathcal{R}^*(-2; m_{\pi_0}^2)$	0.0007473	± 0.0000142	0.0007469	± 0.0000142	0.0007920	± 0.0000011	0.0007924	± 0.0000011
$\mathcal{R}^*(-3; m_{\pi_0}^2)$	0.00005591	± 0.00000126	0.00005591	± 0.00000126	0.00006015	± 0.00000008	0.00006016	± 0.00000008
$\mathcal{R}^\approx(-1; m_{\pi_0}^2)$	0.013609	± 0.000177	0.013556	± 0.000177	0.014018	± 0.000017	0.014071	± 0.000017
$\mathcal{R}^\approx(-2; m_{\pi_0}^2)$	0.0007429	± 0.0000141	0.0007426	± 0.0000141	0.0007873	± 0.0000010	0.0007877	± 0.0000010
$\mathcal{R}^\approx(-3; m_{\pi_0}^2)$	0.00005999	± 0.00000135	0.00005999	± 0.00000135	0.00006456	± 0.00000008	0.00006456	± 0.00000008
$\mathcal{R}^*(-1; 4m_{\pi}^2)$	0.0517876	± 0.0006421	0.0515651	± 0.0006421	0.0531340	± 0.0000674	0.053357	± 0.0000674
$\mathcal{R}^*(-2; 4m_{\pi}^2)$	0.0027449	± 0.0000508	0.0027433	± 0.0000508	0.0028909	± 0.0000037	0.0028925	± 0.0000037
$\mathcal{R}^*(-3; 4m_{\pi}^2)$	0.00019963	± 0.00000448	0.00019962	± 0.00000448	0.00021152	± 0.00000027	0.00021152	± 0.00000027
$\mathcal{R}^\approx(-1; 4m_{\pi}^2)$	0.053085	± 0.000670	0.052860	± 0.000670	0.054582	± 0.000067	0.054808	± 0.000073
$\mathcal{R}^\approx(-2; 4m_{\pi}^2)$	0.0024911	± 0.0000447	0.0024897	± 0.0000447	0.0026288	± 0.0000032	0.0026302	± 0.0000435
$\mathcal{R}^\approx(-3; 4m_{\pi}^2)$	0.0002566	± 0.0000058	0.0002566	± 0.0000058	0.00027612	± 0.00000035	0.00027612	± 0.00000035

the choice of s_0 , which actually should not exceed the threshold $m_{\pi_0}^2$, unless we restrict the analysis to the isovector part with threshold at $4m_{\pi}^2$. Note that actually, the $\mathcal{R}(-n, s_0)$'s vanish for $s_0 \rightarrow 0$. So, if we choose s_0 small enough, the $\mathcal{R}(-n, s_0)$'s can be tuned to be negligible.

Finally, we are able to get the ‘‘lattice extrinsic’’ $\tilde{\mathcal{M}}(-n)$ in terms of quantities accessible with the lattice. The required relations read [18]:

$$\begin{aligned}
\tilde{\mathcal{M}}(-1) &= \Sigma(-1; s_0) - \ln \frac{s_0}{m_{\mu}^2} \mathcal{M}(-1) - \frac{m_{\mu}^2}{s_0} \mathcal{M}(0) + \frac{s_0}{m_{\mu}^2} \mathcal{M}(-2) + \dots \\
\tilde{\mathcal{M}}(-2) &= -\Sigma(-2; s_0) - \ln \frac{s_0}{m_{\mu}^2} \mathcal{M}(-2) - \frac{m_{\mu}^2}{s_0} \mathcal{M}(-1) + \frac{1}{2} \left(\frac{m_{\mu}^2}{s_0} \right)^2 \mathcal{M}(0) \\
&\quad + \frac{s_0}{m_{\mu}^2} \mathcal{M}(-3) + \dots \\
\tilde{\mathcal{M}}(-3) &= \Sigma(-3; s_0) - \ln \frac{s_0}{m_{\mu}^2} \mathcal{M}(-3) - \frac{m_{\mu}^2}{s_0} \mathcal{M}(-2) + \frac{1}{2} \left(\frac{m_{\mu}^2}{s_0} \right)^2 \mathcal{M}(-1) \\
&\quad - \frac{1}{3} \left(\frac{m_{\mu}^2}{s_0} \right)^3 \mathcal{M}(0) + \frac{s_0}{m_{\mu}^2} \mathcal{M}(-4) + \dots
\end{aligned} \tag{34}$$

Adopting the Euclidean ‘‘thresholds’’ (27), for $s_0 = m_{\pi_0}^2$ and $s_0 = 4m_{\pi}^2$, the results up to 3rd order are given in Table 6. These moments again are directly accessible in lattice QCD and

Table 6: The moments $\Sigma(-n; s_0)$ in units 10^{-5} for $s_0 = m_{\pi^0}^2$ in the upper part and for $s_0 = 4m_{\pi}^2$ in the lower part. By $\Sigma^*(-n; s_0)$ we denote the result from (29) and the kernels (30). The version $\Sigma(-n; s_0)$ denotes the result of (31) using the “exact” remainder $\mathcal{R}^*(-n; s_0)$ while $\Sigma^{\approx}(-n; s_0)$ is the result obtained by the truncated expansion (33) including moments up to $n = 4$.

moment	data direct		data HLS channels		HLS model		HLS + remainder	
$\Sigma^*(-1; m_{\pi^0}^2)$	5.46769	± 0.04183	4.58924	± 0.02570	4.57130	± 0.0070	5.44975	± 0.0337
$\Sigma^*(-2; m_{\pi^0}^2)$	1.77639	± 0.01335	1.50224	± 0.00846	1.4969	± 0.0023	1.77105	± 0.0106
$\Sigma^*(-3; m_{\pi^0}^2)$	0.735060	± 0.005500	0.622759	± 0.003517	0.62063	± 0.00095	0.732931	± 0.0043
$\Sigma(-1; m_{\pi^0}^2)$	5.48300	± 0.04122	4.58905	± 0.02604	4.57106	± 0.00697	5.46501	± 0.03350
$\Sigma(-2; m_{\pi^0}^2)$	1.78098	± 0.01310	1.50210	± 0.00842	1.49675	± 0.00228	1.77563	± 0.01054
$\Sigma(-3; m_{\pi^0}^2)$	0.73690	± 0.00542	0.62267	± 0.00350	0.62053	± 0.00094	0.73476	± 0.00432
$\Sigma^{\approx}(-1; m_{\pi^0}^2)$	5.48300	± 0.04122	4.58905	± 0.02605	4.57106	± 0.00697	5.46501	± 0.03352
$\Sigma^{\approx}(-2; m_{\pi^0}^2)$	1.78098	± 0.01310	1.50210	± 0.00842	1.49675	± 0.00228	1.77562	± 0.01054
$\Sigma^{\approx}(-3; m_{\pi^0}^2)$	0.73690	± 0.00542	0.62267	± 0.00350	0.62052	± 0.00094	0.73475	± 0.00432
$\Sigma^*(-1; 4m_{\pi}^2)$	1.02683	± 0.00852	0.83419	± 0.00457	0.82971	± 0.00130	1.02235	± 0.00731
$\Sigma^*(-2; 4m_{\pi}^2)$	0.082682	± 0.000660	0.068218	± 0.000375	0.067882	± 0.000106	0.082346	± 0.000553
$\Sigma^*(-3; 4m_{\pi}^2)$	0.008168	± 0.000064	0.006773	± 0.000037	0.006740	± 0.000011	0.008135	± 0.000053
$\Sigma(-1; 4m_{\pi}^2)$	1.03049	± 0.00847	0.83421	± 0.00502	0.82978	± 0.00127	1.02650	± 0.00716
$\Sigma(-2; 4m_{\pi}^2)$	0.082943	± 0.000621	0.068220	± 0.000366	0.067866	± 0.000106	0.082552	± 0.000553
$\Sigma(-3; 4m_{\pi}^2)$	0.008193	± 0.000061	0.006773	± 0.000037	0.006744	± 0.000010	0.008161	± 0.000064
$\Sigma^{\approx}(-1; 4m_{\pi}^2)$	1.02919	± 0.00844	0.83292	± 0.00499	0.82833	± 0.00127	1.02505	± 0.00730
$\Sigma^{\approx}(-2; 4m_{\pi}^2)$	0.08269	± 0.00062	0.06797	± 0.00036	0.06760	± 0.00011	0.08229	± 0.00059
$\Sigma^{\approx}(-3; 4m_{\pi}^2)$	0.00814	± 0.00006	0.00672	± 0.00004	0.00668	± 0.00001	0.00810	± 0.00006

Table 7: Comparison of the moments $\tilde{\mathcal{M}}(-n)$ as obtained directly via (14) and via the moments expansion (34) for $s_0 = m_{\pi^0}^2$ and $s_0 = 4m_{\pi}^2$ (in units 10^{-5}). Again the $\tilde{\mathcal{M}}^*(-n)$ values are obtained from the timelike integrals over $R(s)$, the other two from moments which are accessible in lattice QCD: the $\Sigma(-n; s_0)$ and $\mathcal{M}(-n)$.

moment	data direct		data HLS channels		HLS model		HLS + remainder	
$\tilde{\mathcal{M}}^*(-1)$	-0.82592	± 0.00516	-0.79611	± 0.00501	-0.80054	± 0.00113	-0.83035	± 0.00167
$\tilde{\mathcal{M}}^*(-2)$	-0.026808	± 0.000294	-0.026644	± 0.000294	-0.027338	± 0.000035	-0.027502	± 0.000035
$\tilde{\mathcal{M}}^*(-3)$	-0.0013160	± 0.0000228	-0.0013149	± 0.0000228	-0.0013847	± 0.0000017	-0.0013858	± 0.0000017
$\tilde{\mathcal{M}}(-1) \Big _{m_{\pi^0}^2}$	-0.84123	± 0.00455	-0.79592	± 0.00535	-0.80030	± 0.00110	-0.84561	± 0.00146
$\tilde{\mathcal{M}}(-2) \Big _{m_{\pi^0}^2}$	-0.02222	± 0.00054	-0.02678	± 0.00034	-0.02749	± 0.00005	-0.02293	± 0.00008
$\tilde{\mathcal{M}}(-3) \Big _{m_{\pi^0}^2}$	-0.003151	± 0.000061	-0.001222	± 0.000007	-0.001279	± 0.000004	-0.003207	± 0.000011
$\tilde{\mathcal{M}}(-1) \Big _{4m_{\pi}^2}$	-0.82828	± 0.00508	-0.79484	± 0.00543	-0.79916	± 0.00110	-0.83260	± 0.00153
$\tilde{\mathcal{M}}(-2) \Big _{4m_{\pi}^2}$	-0.026801	± 0.000339	-0.026896	± 0.000309	-0.027616	± 0.000035	-0.027521	± 0.000037
$\tilde{\mathcal{M}}(-3) \Big _{4m_{\pi}^2}$	-0.001284	± 0.000019	-0.001258	± 0.000021	-0.001324	± 0.000001	-0.001350	± 0.000001

can provide important crosschecks. Again contributions from regions above about 1 GeV are significant for getting reliable estimates.

It is interesting to note that the choice $s_0 = m_{\mu}^2$ leads to a simplification of the formulas (34), particularly the second term with the log is then absent. On the other hand for $s_0 > m_{\mu}^2$ the suppression factors m_{μ}^2/s_0 for the leading moments $\mathcal{M}(0)$, $\mathcal{M}(-1)$ etc. are very welcome in reducing the largest cancellations. Note that the $\tilde{\mathcal{M}}(-n)$'s are an order of magnitude smaller than the corresponding $\mathcal{M}(-n)$'s for a given n (see Table 1).

One observes a strong dependence of the Euclidean integrals $\Sigma(-n; s_0)$ on the infrared cut-off $s_0 = Q_0^2$, reflected by the factor of about 5 between the results for $s_0 = m_{\pi^0}^2$ and $s_0 = 4m_{\pi}^2$. In contrast, the timelike integrals, $\mathcal{M}(-n)$ for example, differ little once the ρ peak is included in the integration range. Changing s_0 from $4m_{\pi}^2$ to $m_{\pi^0}^2$ increases the integral by the $\pi^0\gamma$ contribution, by about 0.5% in $\mathcal{M}(0)$. Typically, the dominant ρ resonance contribution in $R(s)$ in the Adler function $D(Q^2)$ appears completely smeared out leading to a steep monotonic increase at low Q^2 . This high sensitivity on Q_0^2 , corresponding to x_{\min} in the integral (1) where the limit $x_{\min} \rightarrow 0$ is required and where the finiteness of the Adler function slope comes into play. This high sensitivity is one reason why lattice QCD calculations of a_{μ}^{had} are so difficult in reducing uncertainties of the needed extrapolations. The moments $\tilde{\mathcal{M}}(-n)$'s ideally are not dependent on s_0 , but depend on s_0 though truncation errors in the moment expansion. Differences as seen in Table 7 are not really small, but in view of the strong s_0 -dependence of the $\Sigma(-n; s_0)$ mo-

Table 8: Illustrating cancellations of moments according to (34) (in units 10^{-5}). The first term is $\Sigma(-n, s_0)$ the second the log term and the last the truncated $\mathcal{R}(-n, s_0)$ from (33) including moments up to $n = 4$. The second last term, which is proportional to $\mathcal{M}(0)$ in any case overcompensates the $\Sigma(-n, s_0)$ term. Note that uncertainties of the leading terms are easily bigger than some of the subleading contributions.

$n =$	$s_0 = m_{\pi^0}^2$			$s_0 = 4 m_{\pi}^2$		
	1	2	3	1	2	3
$\Sigma(-n, s_0)$	5.449750	-1.771050	0.732931	1.022350	-0.082346	0.008135
$-\ln \frac{s_0}{m_{\mu}^2} \mathcal{M}(-n)$	-0.116384	-0.004412	-0.000252	-0.461658	-0.017501	-0.001000
$\propto \mathcal{M}(-2)$	-	-	-0.005519	-	-	-0.001290
$\propto \mathcal{M}(-1)$	-	-0.145585	0.044602	-	-0.034042	0.002439
$\propto \mathcal{M}(0)$	-6.193043	1.897331	-0.775034	-1.448101	0.103737	-0.009908
$\mathcal{R}(-n, s_0)$	0.014071	0.000788	0.000065	0.054808	0.002630	0.000276
$\tilde{\mathcal{M}}(-n)$	-0.845606	-0.022928	-0.003207	-0.832601	-0.027521	-0.001350

ments, they are quite acceptable. Table 8 illustrates the composition of the $\tilde{\mathcal{M}}(-n)$ predictions in terms of Euclidean objects.

4 How to get the moments $\tilde{\mathcal{M}}(-n)$ directly from lattice QCD data?

We note that the moments $\tilde{\mathcal{M}}(-n)$ are much smaller than the auxiliary moments $\Sigma(-n; s_0)$. There are obviously large cancellations, especially for small s_0 , which enter as inverse power weight factors of the moments $\mathcal{M}(-n)$ to be subtracted from the $\Sigma(-n; s_0)$. In fact these cancellations can be avoided to a large extent. How do we get the moments (26) in terms of lattice data? A direct evaluation of (26) in terms of the Euclidean configuration space correlator, like (22) for the Taylor coefficients, is not available in this case. However, if we assume that $\Pi(Q^2)$ has been determined by a Fourier transform of the Euclidean correlator measured in configuration space, in principle, (26) can be integrated directly without problem when we choose a finite infrared cutoff $Q_0^2 > 0$. Once we are given $\Pi(Q^2)$ itself or as a Taylor series we may proceed as follows: in order to get $\tilde{\mathcal{M}}(-n)$ for a given n , subtract its Taylor expansion to order $n - 1$ from $\Pi(Q^2)$, which defines

$$\Pi(Q^2)_n^{\text{trunc}} \equiv \Pi(Q^2) - \sum_{j=0}^{n-1} (Q^2)^{(j+1)} \Pi_{j+1} \approx \sum_{j=n}^N (Q^2)^{(j+1)} \Pi_{j+1}. \quad (35)$$

As indicated, this also can be done if $\Pi(Q^2)$ is given as a Taylor series to some order $N > n + 1$. In the latter case

$$\Pi(Q^2)_n^{\text{trunc}} / (Q^2)^{(n+1)} \approx \sum_{j=0}^{N-n} (Q^2)^{(j)} \Pi_{n+j+1}, \quad (36)$$

can be Padé improved. We then first evaluate the Taylor moments to order $n - 1$, which provides an expression in terms of normal Taylor moments $\mathcal{M}(-n)$ plus an integral over the subtracted HVP function which, if given as a power series, has to be represented in terms of appropriate Padé approximants in order for the integral to converge at large momenta. We thus obtain:

$$\begin{aligned} \Sigma_n^{\text{trunc}}(-n; Q_0^2) &= - \sum_{j=0}^{n-1} (-1)^{(j+1)} \mathcal{M}(-j) \frac{1}{n-j} (Q_0^2/m_\mu^2)^{j-n} \\ &\quad + \int_{Q_0^2}^{\infty} dQ^2 \left(\frac{m_\mu^2}{Q^2} \right)^{n+1} \left(- \frac{\Pi(Q^2)_n^{\text{trunc}}}{Q^2} \right). \end{aligned} \quad (37)$$

If we subtract one more term for $j = n$ we obtain an UV divergent result or, if regulated with a cutoff Q_1^2 , we get a term

$$\Sigma_n^{\text{trunc}}(-n; Q_0^2) = (-1)^{n+1} \mathcal{M}(-n) (\ln Q_0^2/m_\mu^2 - \ln Q_1^2/m_\mu^2) + \Sigma_{n+1}^{\text{trunc}}(-n; Q_0^2). \quad (38)$$

We thus reproduce the terms involving the moments $\mathcal{M}(-n)$ in (31), which means that evaluating the subtracted HVP function (35) is actually what essentially yields the moments $\tilde{\mathcal{M}}(-n)$, namely,

$$\Sigma_n^{\text{trunc}}(-n, s_0) = (-1)^{n+1} \left(\tilde{\mathcal{M}}(-n) + \ln \frac{s_0}{m_\mu^2} \mathcal{M}(-n) - \mathcal{R}(-n, s_0) \right). \quad (39)$$

Working out additional terms in the Taylor expansion may be as effective and easier. Here we should remember that the remainders $\mathcal{R}(-n, s_0)$ can be made negligible by choosing s_0 small enough, as they vanish in the limit $s_0 \rightarrow 0$. So it turns out that the moments $\tilde{\mathcal{M}}(-n)$, by definition s_0 -independent, are given by the “finite part”:

$$\tilde{\mathcal{M}}(-n) = \lim_{s_0 \rightarrow 0} \left\{ (-1)^{n+1} \int_{s_0}^{\infty} dQ^2 \left(\frac{m_\mu^2}{Q^2} \right)^{n+1} \left(- \frac{\Pi(Q^2)_n^{\text{trunc}}}{Q^2} \right) - \ln \frac{s_0}{m_\mu^2} \mathcal{M}(-n) \right\} \quad (40)$$

This is our master formula for the evaluation of the $\tilde{\mathcal{M}}(-n)$ moments in lattice QCD in particular. In this representation the only purpose of the IR regulator s_0 , to be chosen positive

infinitesimal, is to parametrize the logarithmic singularity. The latter is persisting since the $1/Q^2$ term at low Q has been kept in the truncated HVP function, and remains unaffected by going to the representation by suitable Padé approximants. The latter have to be chosen to behave at large Q^2 in accord with pQCD such that the potential logarithmic UV singularity in (38) will be absent.

What it simply amounts to is the following: let $\Delta\alpha_{\text{had}}(-Q^2) = -\Pi(Q^2) = \sum_{j=0}^N p_j x^{j+1}$ with $x \equiv Q^2/m_\mu^2$ and $p_j = (-1)^j \mathcal{M}(-j)$ from (23). Then we have to consider terms as listed in the following tabular:

moment	Taylor polynomial	term to be subtracted
$\tilde{\mathcal{M}}(-1)$	$p_1 + p_2 x + p_3 x^2 \dots$	$\ln(x_0) \mathcal{M}(-1)$
$\tilde{\mathcal{M}}(-2)$	$p_2 + p_3 x + p_4 x^2 \dots$	$\ln(x_0) \mathcal{M}(-2)$
$\tilde{\mathcal{M}}(-3)$	$p_3 + p_4 x + p_5 x^2 \dots$	$\ln(x_0) \mathcal{M}(-3)$
\dots	\dots	\dots

Then take the [1,2] Padé for example of the polynomial in the list and integrate $(-1)^{n+1} [1, 2](x)/x$ over x from $x_0 = s_0/m_\mu^2$ to infinity and subtract the IR sensitive term $\ln(x_0) \mathcal{M}(-n)$ in order to get $\tilde{\mathcal{M}}(-n)$. For the [1,1] and [2,2] Padés, the integral obviously diverges.

This is our main results: the Mellin-Barnes moment expansion can be implemented in a surprisingly straightforward manner by the evaluation of (16) or (22) for the Taylor moments $\mathcal{M}(-n)$ and by the evaluation of (40) for the log suppressed moments $\tilde{\mathcal{M}}(-n)$. A detour via the moments $\Sigma(-n, s_0)$ and the remainders $\mathcal{R}(-n, s_0)$ at the end turns out to be superfluous, but may serve for crosschecks.

We have tested the truncated HVP approach by using $\Delta\alpha_{\text{had}}(-Q^2)$ based on a world average (WA) compilation of the e^+e^- data (as available from [46]) together with the related Taylor moments⁷ to order $n = 12$, which allows us to calculate Padé approximants [n-1,n] and [n,n] up

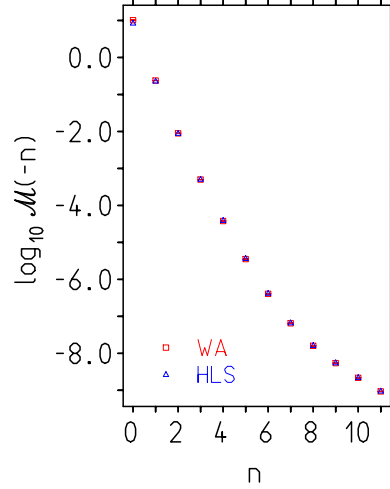


Figure 7: The $\log_{10} \mathcal{M}(-n)$ are shown for $n = 0, \dots, 11$. The HLS model moments for the larger n values agree well with the e^+e^- -data estimates, within uncertainties. Error bars are barely visible on top of the marks.

to $n = 4$. In Fig. 7 we display the logarithm of the moments used in our analysis. The Padéized Taylor polynomials multiplied by x (to get ride of the $1/x$ singularity) are displayed in Fig. 8 and show a nice convergence. For the $[n,n]$ Padés we need a high energy cutoff, above which we use the corresponding truncated HVP function $\Delta\alpha_{\text{had}}(-Q^2)$. The $[n-1,n]$ Padés alone can be integrated without a high energy cutoff. In any case, we think our tables shed light on how

⁷For the Taylor coefficients for the WA compilation and the HLS model prediction we find

n	WA compilation			HLS model		
0	$1.01962131E + 01$	\pm	$6.693577E - 02$	$8.60436543E + 00$	\pm	$1.303549E - 02$
1	$2.38190432E - 01$	\pm	$1.257508E - 03$	$2.31974285E - 01$	\pm	$3.137495E - 04$
2	$8.89142868E - 03$	\pm	$5.749533E - 05$	$8.97346405E - 03$	\pm	$1.138840E - 05$
3	$4.99117005E - 04$	\pm	$4.018536E - 06$	$5.14676918E - 04$	\pm	$6.561512E - 07$
4	$3.78809709E - 05$	\pm	$3.333508E - 07$	$3.95581883E - 05$	\pm	$5.245059E - 08$
5	$3.53345581E - 06$	\pm	$2.971228E - 08$	$3.70101838E - 06$	\pm	$6.216865E - 09$
6	$4.06928851E - 07$	\pm	$2.867316E - 09$	$4.23990709E - 07$	\pm	$1.378845E - 09$
7	$6.51188814E - 08$	\pm	$4.102998E - 10$	$6.72641010E - 08$	\pm	$4.547703E - 10$
8	$1.59771291E - 08$	\pm	$1.260996E - 10$	$1.64295040E - 08$	\pm	$1.722887E - 10$
9	$5.43416738E - 09$	\pm	$5.033454E - 11$	$5.58818049E - 09$	\pm	$6.967189E - 11$
10	$2.17223798E - 09$	\pm	$2.125434E - 11$	$2.23581201E - 09$	\pm	$2.941683E - 11$
11	$9.33132065E - 10$	\pm	$9.276033E - 12$	$9.60971183E - 10$	\pm	$1.283852E - 11$

We refer to the comments at the end of Sect. 2 for what concerns the difference in the evaluations of the two sets of moments which ideally should agree for the higher moments.

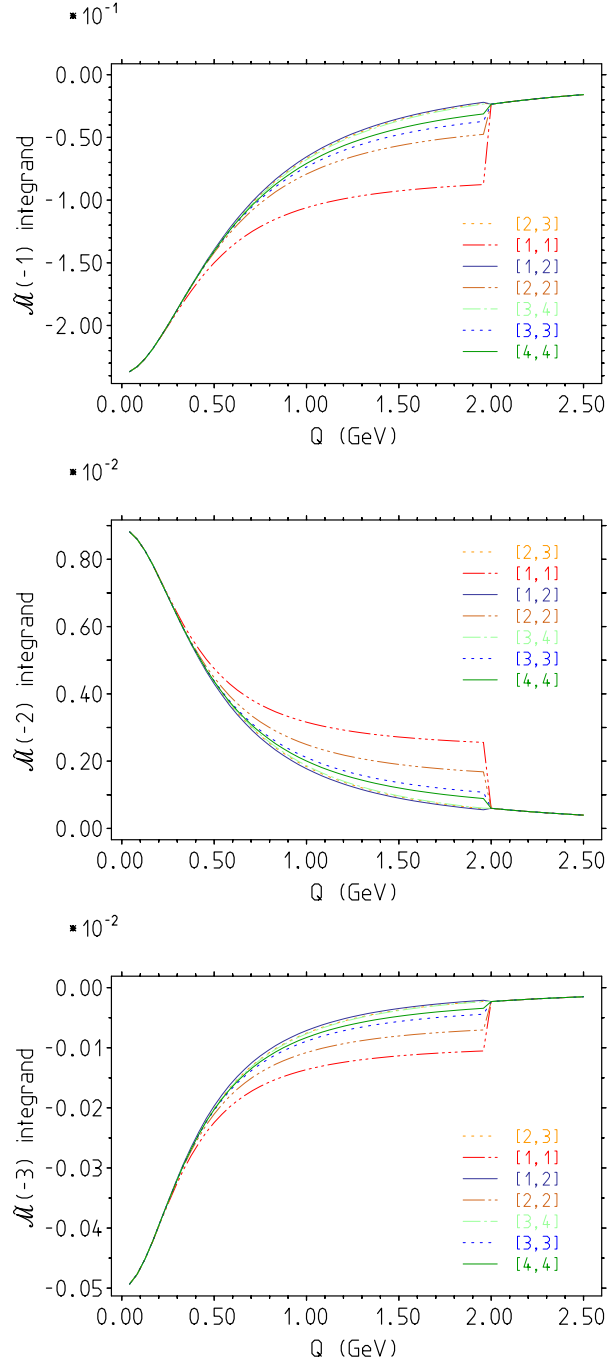


Figure 8: The integrands of Eq. (40) with an extra weight factor $x = Q^2/m_\mu^2$ for $\tilde{\mathcal{M}}(-n)$ ($n = 1, 2, 3$) as a function of Q and with a Padé cutoff at 2 GeV. One can see that the Padé pairs $[n-1,n]+[n,n]$ ($n = 1, 2, 3, 4$) nicely converge.

the MBM approach works in Euclidean space, where it is by far not as straightforward as in the timelike domain. In case $\Pi(Q^2)$ is given as a Taylor expansion, at the end it turns out that also the moments $\tilde{\mathcal{M}}(-n)$ are determined by the normal Taylor coefficients, just the indices get shifted according to (36). Interestingly, the MBMs $\mathcal{M}(-n)$, up to normalization, are directly given by the Taylor coefficients Π_n and there is no integration to be performed and thus no need for a Padéization. In contrast, the log suppressed MBMs $\tilde{\mathcal{M}}(-n)$ are obtained by integrating the truncated HVP, and if the latter is given as a Taylor series, a Padé improvement is necessary. After all the $\tilde{\mathcal{M}}(-n)$'s can also be obtained alone in terms of moments which can be evaluated in configuration space via (22).

As already mentioned earlier, by choosing $s_0 = m_\mu^2$, i.e. $x_0 = 1$, we get rid of the subtraction term! In this representation there is no reason to choose m_μ^2/s_0 small in order to suppress the larger low- n moments $\mathcal{M}(-n)$, because the subtraction is done on the level of the integrand in which case these moments no longer appear. However, the remainders evaluated to be $\mathcal{R}(-n, m_\mu^2) = 8.6541(0.0555) \times 10^{-3}, 4.8016(0.0314) \times 10^{-4}, 3.7880(0.0330) \times 10^{-5}$ for $n = 1, 2, 3$ in units 10^{-5} are not negligible yet for $s_0 = m_\mu^2$.

Note that uncertainties can barely be evaluated if we only are using the lower bound [n-1,n] approximations, for which the integrals converge. In order to get a handle to estimate the uncertainty we cannot circumvent the consideration of the upper bound [n,n] approximations as well. As the integrals of the latter do not converge, we need to apply an UV cutoff, as we did when deriving the results for a_μ^{had} presented in Table 3. We may then take the mean and the deviation for pairs [n-1,n]+[n,n] and should get reasonable error estimates for sufficiently large n , besides a small additional contribution from the high energy tail, where we use $\Delta\alpha_{\text{had}}(-Q^2)$, as obtained from a world average compilation of the e^+e^- data. The results obtained for $\tilde{\mathcal{M}}(-n)$ for $n = 1, 2, 3$ based on the [3,4]+[4,4] Padé approximants are displayed in Fig. 9, together with the other $\tilde{\mathcal{M}}(-n)$ determinations presented before.

While the $\tilde{\mathcal{M}}$'s can be neatly determined in terms of experimental data or HLS predictions, the calculation of the $\tilde{\mathcal{M}}$'s from purely Euclidean LQCD data turns out to be problematic when we attempt to use (34) together with (26). One problem is the choice of s_0 , depending on the method applied, we observe a substantial spread of the results. The most stable results one obtains are for $s_0 = 4m_\pi^2$. The methods based on the subtraction of the moment expansion from the Σ integrals are, in a way, complementary to the method based on integrating the integrand after subtraction of the moment expansion (truncated HVP version). The first works better for the larger s_0 values, but is of limited reliability because of the delicate cancellation pattern illustrated in Table 8. In contrast, for sufficiently high Padé approximants, the truncated HVP method works perfectly and, for sufficiently low finite s_0 , without the need to know the remainders $\mathcal{R}(-n, s_0)$.

The Padé approximants obtained from a low energy expansion in general fail to be reliable at higher momentum transfer. It looks bold to predict what happens above the ρ resonance from

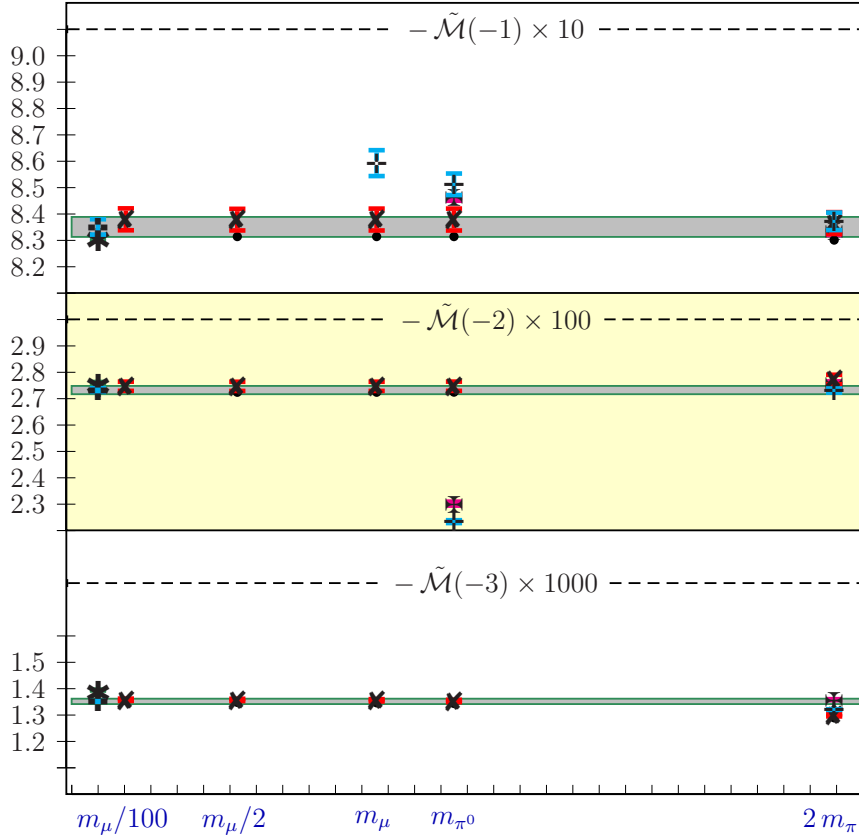


Figure 9: The dependence of the moments $\tilde{\mathcal{M}}(-n)$ evaluated via the truncated HVP on $\sqrt{s_0}$, together with the direct (by definition s_0 -independent) determination in terms of data (\blacksquare), which also determines the error bands shown. The results obtained via (34) listed in Table 7 are also displayed (marked by \boxtimes , the s_0 -independent “HLS + remainder” evaluation by \blackstar). Values obtained via the Euclidean definition of $\Sigma(-n; s_0)$ (marked by \blacklozenge), within the ranges displayed, could be evaluated reliably only for the largest s_0 , where they agree with the results collected in Table 7. The evaluation via the truncated HVP yield the results marked by a \bullet for the lower bound [3,4] Padés. The upper bound Padés $[n,n]$ $n=1,2,3,4$ lead to divergent integrals, if no cutoff is applied. With a cutoff of 2 GeV the $[3,4]+[4,4]$ averages, marked by a \blackstar , for $\tilde{\mathcal{M}}(-1)$ moderately differ from the [3,4] Padés without cutoff, while for $\tilde{\mathcal{M}}(-2)$ and $\tilde{\mathcal{M}}(-3)$ the values agree within uncertainties. The tilt in the s_0 -dependence of the Padé estimates based on (40), where the remainders $\mathcal{R}(-n; s_0)$ have been dropped as they vanish in the limit $s_0 \rightarrow 0$, completely disappears if one is including the remainders $\mathcal{R}(-n; s_0)$ (marks \bullet/\blackstar , mostly not distinguishable). For the closest point at $s_0 = m_\mu^2/100$ the remainder is negligible such that (40) yields the correct result for finite but small enough s_0 . The lower order Padé pairs yield very similar results to the ones shown with larger errors, however.

Table 9: A numerical consistency test: Comparison of the timelike with the spacelike evaluations of the moments $\Sigma(-n; s_0)$ and remainders $\mathcal{R}(-n; s_0)$ in units 10^{-5} . Here we use moments obtained for the compilation used to evaluate $\Delta\alpha_{\text{had}}(-Q^2)$ for $s_0 = m_{\pi_0}^2$ in the upper part and for $s_0 = 4m_{\pi}^2$ in the lower part. By $\Sigma^*(-n; s_0)$ and $\mathcal{R}^*(-n; s_0)$ we denote the result from (29) and (32), respectively. The version $\Sigma^{\approx}(-n; s_0)$ and $\mathcal{R}^{\approx}(-n; s_0)$ denote the LQCD appropriate evaluations of (26) and the truncated expansion (33) including moments up to $n = 4$.

moment	Σ^* (29)		Σ^{\approx} (26)		\mathcal{R}^* (32)		\mathcal{R}^{\approx} (33)	
$n = 1$	5.5032	± 0.0380	5.4993	± 0.0366	0.013895	± 0.000089	0.013901	± 0.000089
2	1.7882	± 0.0121	1.7869	± 0.0116	0.00076861	± 0.00000615	0.00076410	± 0.00000495
3	0.7400	± 0.0050	0.73944	± 0.00479	0.00005762	± 0.00000051	0.000061822	± 0.000000539
1	1.0328	± 0.00780	1.03228	± 0.00749	0.052864	± 0.000337	0.054193	± 0.000355
2	0.083181	± 0.000603	0.083108	± 0.000581	0.0028220	± 0.0000222	0.0025609	± 0.0000150
3	0.0082175	± 0.0000588	0.0082098	± 0.0000566	0.00020577	± 0.00000182	0.00026439	± 0.00000230

information which zooms into what is happening below it, however, as illustrated by Fig. 8, this is precisely what seems to work⁸. If we want to avoid the need of Padé approximations the method based on (31) solved for $\tilde{\mathcal{M}}$ together with the expansion (33) is adequate. This method requires an optimized choice of s_0 , because moments enhanced by powers of m_{μ}^2/s_0 appear together with higher moments weighted by factors s_0/m_{μ}^2 in (34). For lower s_0 values the cancellations in (34) grow and may cause numerical problems. Fortunately, the moments $\Sigma(-n; s_0)$ directly evaluated via their definition (26), agree rather well with their estimations in terms of timelike data via (29), as it should be. This can be concluded from the numerical crosscheck presented in Table 9. Concerning methods which require Padé approximations to be used as a tool for the extrapolation towards higher momenta we have to be aware that the HVP “modeling” never is really good, because $\Pi(Q^2)$ grows logarithmically and not powerlike. The need of the truncated HVP in the evaluation of the $\tilde{\mathcal{M}}$ ’s also reveals, that one needs more Taylor moments than we might have expected in order to reach a desired precision⁹. We should be aware also of the fact that the MBM estimation (15) of a_{μ}^{had} is very sensitive to the $\tilde{\mathcal{M}}$ ’s as illustrated in Fig. 10. It reveals that the MBM method has its weak points here.

⁸We quote Numerical Recipes commenting an example with five terms of a power series in x : Why does this work? Are there not other functions with the same first five terms in their power series, but completely different behavior in the range (say) $2 < x < 10$? Indeed there are. Padé approximation has the uncanny knack of picking the function *you had in mind* from among all the possibilities. *Except when it doesn't!* That is the downside of Padé approximation: it is uncontrolled. There is in general no way to tell how accurate it is, or how far out in x it can usefully be extended. It is a powerful, but in the end still mysterious, technique [47].

⁹Considering the truncated HVP required for the calculation of $\tilde{\mathcal{M}}(-n)$ we loose n Taylor coefficients and since we need [n-1,n] and [n,n] type Padé approximants, which requires $2n + 1$ coefficients, a [4,4] Padé for $\tilde{\mathcal{M}}(-3)$ requires 12 Taylor coefficients.

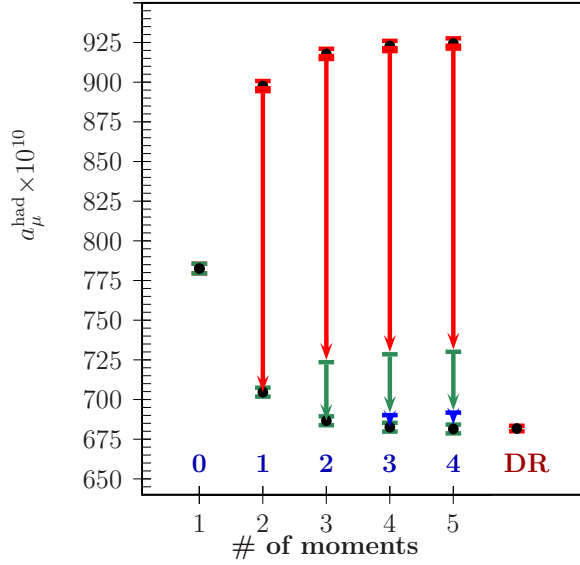


Figure 10: This graph illustrates the relevance of the log suppressed moments $\tilde{\mathcal{M}}(-n)$ in calculating a_μ^{had} via (15). As we know the starting point of the MBM expansion overestimates a_μ^{had} substantially. All the normal (Taylor) moments $\mathcal{M}(-n)$ are positive and are corrections in the “wrong direction”. Thus the $\tilde{\mathcal{M}}(-n)$ moments are the ones not only to compensate the $\mathcal{M}(-n)$ contributions, but also the ones which have to correct for the overestimation we start with. This shows the importance to have precise estimations of the $\tilde{\mathcal{M}}(-n)$ ’s. The high points in the graph are the ones given by the series (15) where the $\tilde{\mathcal{M}}$ ’s are dropped, while the lowest ones represent the full result (15). The $\tilde{\mathcal{M}}$ ’s are included consecutively for $n = 1, 2, 3$ (red, green, blue) from top to bottom. The $\tilde{\mathcal{M}}(-4)$ contribution is too small to be displayable here.

Although the Mellin-Barnes moments approach shows excellent convergence, it looks to be quite elaborate as one has to determine quite a number of moments in order to get reliable results. As advocated in [48, 49] (also see [12] and references therein), the best and simplest check of lattice QCD data is to compare the results with the Adler function as it enters in the representation (1) and as it actually has been performed in [8], recently. An up-to-date evaluation of the “experimental” Adler function $D(Q^2)$ is available via the link [13]. We remind that the Adler function asymptotically tends to a constant at high Q^2 , which means that Padé approximants applied to the Adler function in principle can be properly matched to QCD asymptotics. This is another advantage of working with $D(Q^2)$ rather than with $\Pi(Q^2)$ (compare Figs. 5 and 6 in this context).

5 BHLS Evaluation of the I=1 Component of the HVP

Most LQCD calculations of the Euclidean HVP function attempt to derive the isovector part as the leading contribution in a first step. It is, therefore, desirable to have an “experimental” counterpart, which allows one to compare results. However, on the data side, a separation of the I=1 part from the e^+e^- data as well as its determination in terms of the τ data is not straightforward (missing channels, electromagnetic effects). A corresponding evaluation in the HLS model looks to be much more reliable and is presented in this section.

5.1 Reconstruction of HVP From Normal Fits & τ +PDG

The model results referred to in the above Sections have been all derived by running in the standard mode the broken HLS (BHLS) model as defined in [50] and recently improved in [41]. This improvement deals with the need to properly account, in the fitting procedure, for the special character of the overall normalization uncertainties strongly affecting the most recent $e^+e^- \rightarrow \pi^+\pi^-$ data samples. This last study also provided a new update of the BHLS analysis [42] by including the spectra recently published by KLOE [24] and BESIII [26].

The standard running mode of the BHLS fit procedure is a *global* fit which covers simultaneously all the physics channels embodied within the BHLS model. As already noted, these represent the six e^+e^- annihilation channels to $\pi^+\pi^-$, $\pi^0\gamma$, $\eta\gamma$, $\pi^+\pi^-\pi^0$, K^+K^- and $K_L K_S$, the $\tau \rightarrow \pi^\pm\pi^0\nu$ decay and a few additional pieces of light meson decay information [50]. The yielded fit quality is high [41] as reflected by the probability and the average χ^2 per data point for all the physics channels addressed.

For the present purpose, it is worth noting that the (BHLS) model description closely follows the information which can be directly derived from the existing experimental data, as well

reflected by the two central data columns in Tables 1 and 2 and also by Fig. 7; this indicates that the model dependence of the numerical results should be quite marginal.

The purpose of the present work is to relate phenomenology and the calculations which can be achieved within the framework of lattice QCD. Our aim is twofold : compare LQCD predictions with data on the one hand, and on the other hand, initiate – with BHLS – examining the relevance of effective models versus LQCD. For this purpose, Figure 5 in [17] clearly indicates that model predictions for a_μ^{had} [40, 41] derived using Effective Lagrangians or elaborate data handling (as [51]), are in fair agreement with LQCD estimates; how this general agreement will evolve with the increasing accuracy of lattice computations is an important issue to follow.

Nevertheless, going closer to what can be derived within the lattice computation framework as it presently stands is certainly valuable. For instance, if one could motivatedly single out the isovector component of a_μ^{had} , its comparison with LQCD predictions could be directly performed. In this prospect, identifying (and switching off) the IB effects at work in the experimental data and splitting up reliably the Isospin 0 and 1 components of a_μ^{had} is of particular relevance. Obviously, such a program can hardly be performed directly with the measured data, while it looks in the realm of effective models. As the BHLS model accounts well for a large amount of experimental data in various physics channels, such a procedure deserves to be attempted with it.

5.2 Isospin Breaking and the τ +PDG Approach

It has been shown [41, 42, 38] that the (dominant) contribution of the $\pi^+\pi^-$ intermediate state to a_μ^{had} can be well estimated¹⁰ without using the $e^+e^- \rightarrow \pi^+\pi^-$ experimental spectra. The pion form factor $F_\pi^\tau(s)$ in the $\tau \rightarrow \pi^\pm\pi^0\nu$ decay can be almost exactly identified with the hypothetical isospin symmetric pion form factor $F_\pi(s)$; indeed, as far as the pion form factor is concerned, IB effects generated by the pion mass splitting are located only in the pion loop entering the charged ρ propagator¹¹.

The issue solved by BHLS is to provide a *global* framework and a fitting tool able to derive the pion form factor $F_\pi^e(s)$ in the e^+e^- annihilation from fitting $F_\pi^\tau(s)$ and a few pieces of decay information carrying the isospin breaking (IB) content at work in $e^+e^- \rightarrow \pi^+\pi^-$. These IB pieces of information are¹² :

- (i) the $V \rightarrow \pi^+\pi^-$ partial widths for $V = \omega, \phi$,

¹⁰In the energy range limited upward by 1.05 GeV, the domain of validity of the HLS model [52]. This is not a real limitation to compare with precise LQCD estimates.

¹¹As also for the Kaon mass splitting in the Kaon loops.

¹²Actually, the listed pieces of information for the ϕ meson are used in the standard running of the BHLS fitting code because no published experimental dipion spectrum covering the ϕ mass region is presently available.

- **(ii)** the products $\Gamma(V \rightarrow \pi^+\pi^-) \times \Gamma(V \rightarrow e^+e^-)$ for $V = \omega, \phi$,
- **(iii)** the $\rho^0 \rightarrow e^+e^-$ partial width,

which can be extracted from the Review of Particle Properties (RPP) [53]. Of course, $F_\pi^\tau(s)$ depends on the $[\pi^\pm\pi^0]$ (and $[K^\pm K^0]$) loop(s), but the prediction for $F_\pi^e(s)$ accounts automatically for its dependence upon the $[\pi^+\pi^-]$ (and $[K^+K^-], [K^0\bar{K}^0]$) loop(s) with thresholds at their physical masses.

In principle, the $\rho^0 \rightarrow e^+e^-$ information is already contained inside the other channels encompassed within the BHLS framework and could be avoided; however, as this coupling has a marginal impact in these other processes, a more precise information is mandatory.

The results which summarize the τ +PDG prediction for $F_\pi^e(s)$ are shown in Fig. 11 and deserve some comments about how well IB effects accommodate the BHLS framework. The upper three panels display the τ +PDG predicted $F_\pi^e(s)$ function together with the $\pi^+\pi^-$ data; one should keep in mind that all the $\pi^+\pi^-$ experimental spectra are *excluded from the BHLS global fit* when running in the τ +PDG mode. As noted in [42, 41], the picture which arises from these plots is, at the observed level, surprisingly successful, showing that the IB information requested by BHLS is carried solely by the data pieces listed above in **(i–iii)**. This statement is enforced by the middle sequence of panels in Fig. 11 where one has displayed the plots of the difference between the experimental data and the τ +PDG prediction of the BHLS model; indeed, after the canonical¹³ correction for the global scale uncertainties, the "pseudo-residual" distributions (they do not follow from a fit involving the measured $\pi^+\pi^-$ spectra) are shown quite satisfactorily spread around the zero level; this is especially striking for the KLOE or BESIII spectra¹⁴ which are statistically free of any correlation with any of the data samples or decay information running in the τ +PDG fit mode.

In order to substantiate the quality of the prediction, the lowest sequence of panels shows the corresponding (real) residual distributions¹⁵. These are as well centered around the zero residual level as the pseudo-residuals. The improvement provided by the global fit compared to the τ +PDG fit mode is in the dispersal of the residuals, larger for the pseudo-residuals than for

¹³ Without going into details and references which can be found in [41], let us sketch how a global scale uncertainty should be accommodated. For any function $f(s)$, the unbiased residuals $\Delta f(s)$ are, in principle, derived from the raw residuals $f_{exp}(s) - f_{fit}(s)$ via $\Delta f(s) = f_{exp}(s) - f_{fit}(s) - \lambda f_{true}(s)$, where λ is the scale uncertainty which can be derived using fit results [42]. When $f_{true}(s)$ is unknown – which is a rather common situation – an iterative fit procedure has been shown to lead to a $f_{fit}(s)$ close enough to $f_{true}(s)$ that $f_{exp}(s) - (1 + \lambda)f_{fit}(s)$ is a very good approximation of $\Delta f(s)$.

¹⁴The decay information **(i–iii)** extracted from the RPP [53] is driven by the CMD2 and SND pion form factor spectra [19, 20, 21] and totally independent of their analogs from KLOE or BESIII.

¹⁵By real residuals, we mean the normalized differences¹³ between the e^+e^- data and the $F_\pi^e(s)$ derived from the global fit involving also the $e^+e^- \rightarrow \pi^+\pi^-$ data samples.

Table 10: The LO-HVP contribution in terms of moments in units of 10^{-10} . The rightmost pair of data columns are derived by dropping out the effects generated by the Isospin breaking (IB) terms. The integration is performed over the usual BHLS range, *i.e.* from m_{π^0} to 1.05 GeV.

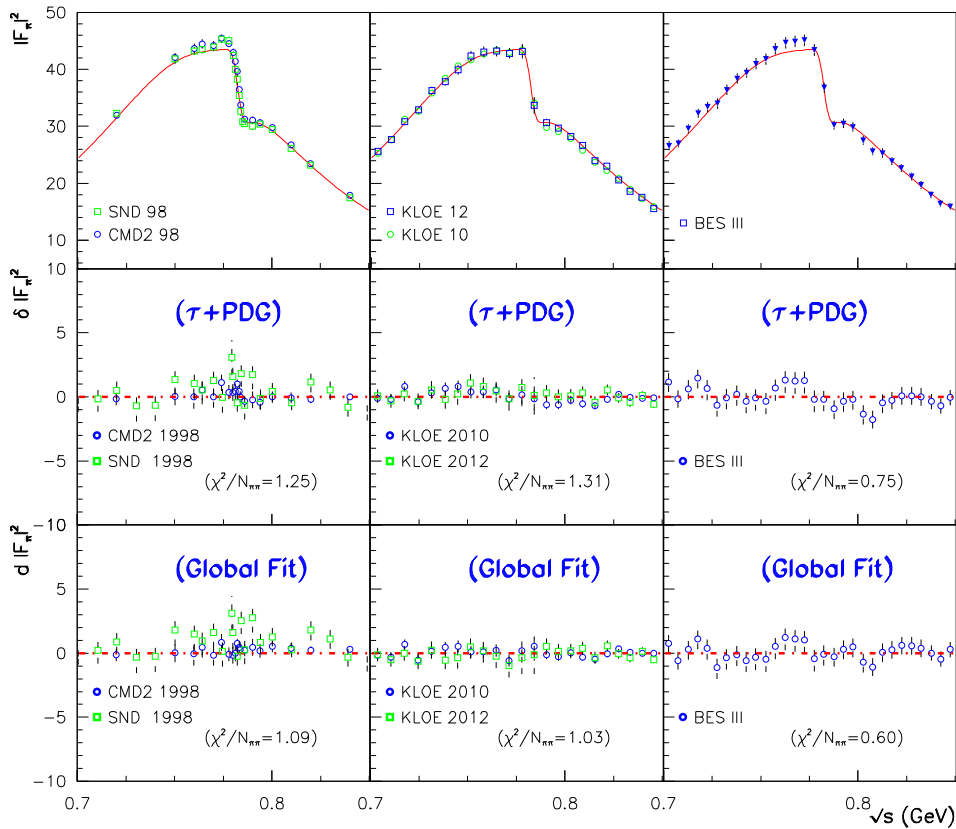
	Exp. data HLS scope	HLS Fits		HLS Fits (IB terms removed)	
		Standard Fit	τ + PDG	γ & I=0 & I=1	γ & I = 1
$a_{\mu}^{\text{had}}(0)$	668.00 ± 3.83	666.22 ± 1.01	665.27 ± 1.70	631.95 ± 0.95	552.15 ± 0.75
$a_{\mu}^{\text{had}}(1)$	594.11 ± 3.56	592.50 ± 0.90	591.72 ± 1.47	562.08 ± 0.84	489.66 ± 0.67
$a_{\mu}^{\text{had}}(2)$	576.51 ± 3.41	574.64 ± 0.88	573.85 ± 1.44	545.08 ± 0.83	473.49 ± 0.65
$a_{\mu}^{\text{had}}(3)$	572.65 ± 3.35	570.58 ± 0.88	569.86 ± 1.45	541.25 ± 0.82	469.70 ± 0.64
$a_{\mu}^{\text{had}}(4)$	571.59 ± 3.33	569.41 ± 0.87	568.76 ± 1.42	540.16 ± 0.82	468.62 ± 0.64
a_{μ}^{had}	570.68 ± 3.67	568.95 ± 0.89	568.11 ± 1.45	539.56 ± 0.81	468.03 ± 0.65

the real residuals, as evidenced by comparing the respective average χ^2 's which can be read off the various panels in Figure 11. This improvement – even if small – is not really unexpected as 5 (actually¹² 3) IB pieces of information are replaced by $\simeq 320$ data points.

Stated otherwise, relying on the dipion spectra collected by ALEPH, CLEO and Belle and on some decay data, one yields a precise determination of $F_{\pi}^e(s)$ and a good estimation of $a_{\mu}^{\text{had}}(\pi^+\pi^-)$, as shown in [41, 38]. The τ +PDG approach of BHLS provides results displayed in Table 10.

The first data column in this Table reproduces the integration of the experimental data covered by BHLS and the second data column shows the results coming from integrating the solution to the standard (normal) fit; these have already been given in the two central columns of Table 2 and are reminded for convenience. The third data column in Table 10 displays the results derived by running the fit procedure in the τ +PDG mode just sketched. One should note the closeness of the corresponding numbers in the second data column (derived by fitting the rich set of $\pi^+\pi^-$ data samples from the CMD–2, SND, KLOE and BESIII Collaborations) and the third data column (relying on the τ data and some limited RPP information). The really new information here is to remark that the statistics of the $\pi^+\pi^-$ data samples allows to improve the uncertainty by $\simeq 50\%$, while the central values shifts by less than 1σ . Another improvement is that the distributions from which the central values for the $a_{\mu}^{\text{had}}(n)$'s and their standard deviations are extracted are much closer to Gaussians in the standard mode than when running the

Figure 11: The pion form factor (PFF) data compared to the τ +PDG prediction and to the global fit. The upper sequence displays the τ +PDG prediction $F_{\pi}^e(s)$ for the PFF in e^+e^- annihilations together with the indicated data superimposed. The middle sequence displays the difference between this prediction and the data. The lower sequence shows the (true) residual plots, e.g. the difference between the global fit solution to $F_{\pi}^e(s)$ and the data. Both kinds of residuals are corrected (see text). The average χ^2 distances of the prediction and of the fit solution to the data samples are indicated in each panel.



τ + PDG mode¹⁶.

5.3 Inverting The τ + PDG Approach

The τ + PDG approach, which allows to plug IB effects within the isovector part of the pion form factor $F_\pi(s)(= F_\pi^\tau(s))$ and in the photon HVP (a_μ^{had}), provides also a way back to restore Isospin symmetry in the cross sections used to evaluate the $a_\mu^{\text{had}}(n)$'s and in the MBM moments (or in the Taylor expansion series coefficients).

As LQCD calculations generally focus on the I=1 part of the HVP and neglect IB effects, one can expect BHLS to extract from data quantities which can be the most directly compared with LQCD predicted HVP values and moments. Since the higher moments ($n \geq 2$) in the moment analysis are given by the HLS accessible contributions within uncertainties (see Table 1), the corresponding LQCD analysis concerns just the range of validity of the BHLS model.

In order to construct the requested amplitudes, the fit parameter values and the parameter error covariance matrix should be those of the global fit in the standard mode running where all data are submitted to fit, as in [41] for instance. Indeed, the standard fit is supposed to provide the basic parameters of the unbroken HLS model (like the parameters named g , a , the FKTUY parameters [54, 52] c_i, \dots), beside the strictly speaking breaking parameters.

Then, restoring Isospin conservation is performed first by switching off the IB parameter¹⁷ while keeping the others. Isospin symmetry also imposes to cancel out the I=1 components inside the ω and ϕ mesons; this turns out to forbid the $\omega/\phi \rightarrow \pi^+\pi^-$ decays. Within BHLS, these decays are generated via the difference between the charged and neutral Kaon loops; then, as restoring Isospin conservation implies to impose $m_{K^\pm} = m_{K^0}$, this loop difference should be canceled out, preventing the $\rho^0 - \omega$ and $\rho^0 - \phi$ dynamical mixings; so, the vanishing of the mixing angles [50] $\alpha(s)$ and $\beta(s)$ cancels out the $\omega/\phi \rightarrow \pi^+\pi^-$ couplings; however, the dynamical mixing in the $\omega - \phi$ sector still survives as it is driven by the sum of the Kaon loops.

At this stage, the BHLS Isospin conserved amplitudes contain well defined I=0 (tagged by the couplings to either of the ω or ϕ mesons) and I=1 (tagged by the coupling to ρ^0) components; the direct coupling of photons to the hadronic final state also survives in our amplitudes.

The results for $a_\mu^{\text{had}}(n)$ referring to the two configurations named resp. $\gamma+(I=0)+(I=1)$ and

¹⁶The distribution obtained by sampling the fit parameters on a multidimensional Gaussian with the fit covariance matrix are very close to 'perfect' Gaussians in the standard mode running, despite non-linearities; in the τ + PDG mode running, small non-Gaussian tails distort the parameter distributions; referring to the last line of Table 10, the numerical estimate of the mean value and r.m.s. of the distribution gives 568.28 ± 2.31 instead of its Gaussian fit result 568.11 ± 1.45 .

¹⁷These are essentially the model parameters [50] named Δ_A, Δ_V . Taking the pion form factor in the τ decay as reference, implies to let Σ_V vary within its allowed range.

$\gamma+(I=1)$ are derived by using generated Monte Carlo data samples and the results are given in the last two data columns of Table 10. In this Table the integration is performed from m_{π^0} to 1.05 GeV. Moreover, the correlations between the parameters considered and those which are canceled out are accounted for at the Monte Carlo generation level.

The last line in Table 10 indicates that IB effects can be estimated to 29.39×10^{-10} , which represents 5.2% of a_μ^{had} . The last two data columns yield $a_\mu^{\text{had}}(I = 0, s < 1.05 \text{ GeV}) = 71.53 \times 10^{-10}$, *i.e.* 12.6% of a_μ^{had} . So, together, IB and I=0 effects amount to 17.8 % of a_μ^{had} in the HLS energy range.

Dealing with the photon terms is a more delicate matter and might introduce a strong model dependence while the value for $a_\mu^{\text{had}}(\gamma \& [I = 1], s < 1.05 \text{ GeV})$ in Table 10 can reasonably be trusted.

Indeed, while IB is canceled out, the photon coupling to a pion pair within BHLS is $g_{\gamma\pi\pi}^{\text{HLS}} = (1 - a_{\text{HLS}}/2)e$, which numerically gives $g_{\gamma\pi\pi}^{\text{HLS}} \simeq -0.25e$; in standard VMD models one assumes $g_{\gamma\pi\pi}^{\text{HLS}} = 0$ (*i.e.* $a_{\text{HLS}} = 2$) while models based on scalar QED (as [61, 40]) yield good fits with $g_{\gamma\pi\pi} = e$. As such kinds of models can satisfactorily describe the pion form factor in the e^+e^- annihilation, one can legitimately suspect that some kind of numerical conspiracy is at work within fits when sharing physical effects between $\gamma \rightarrow \text{hadr.}$ and $\rho^0 \rightarrow \text{hadr.}$. With this proviso in mind, we give below the outcome of setting $g_{\gamma\pi\pi}^{\text{HLS}} = 0$ within our model results while reconstructing the amplitudes.

Table 11: Specific channel contributions to the I=1 a_μ^{had} . The LO-HVP contribution in terms of moments in units of 10^{-10} . One observes that the effect of the full I=1 amplitude is almost saturated by the $\pi^+\pi^-$ channel and a very small correction is provided by the $\pi^0\gamma$ and $\eta\gamma$ channels. In the last data column, the direct coupling $\gamma \rightarrow \text{hadr.}$ is canceled out together with the final state radiation (FSR) effects .

	All HLS Channels	$a_\mu^{\text{had}}(I = 1 \& \gamma)$		$a_\mu^{\text{had}}(I = 1) \& \text{no } \gamma$ $\pi^+\pi^-$
		$\pi^+\pi^-$	$\pi^+\pi^- + \pi^0\gamma + \eta\gamma$	
$a_\mu^{\text{had}}(0)$	552.15 ± 0.75	551.81 ± 0.75	552.14 ± 0.75	562.45 ± 0.78
$a_\mu^{\text{had}}(1)$	489.66 ± 0.67	489.37 ± 0.67	489.65 ± 0.67	498.55 ± 0.68
$a_\mu^{\text{had}}(2)$	473.49 ± 0.65	473.20 ± 0.64	473.48 ± 0.65	481.60 ± 0.67
$a_\mu^{\text{had}}(3)$	469.70 ± 0.64	469.42 ± 0.64	469.70 ± 0.63	477.51 ± 0.66
$a_\mu^{\text{had}}(4)$	468.62 ± 0.64	468.34 ± 0.64	468.61 ± 0.64	476.35 ± 0.66
a_μ^{had}	468.03 ± 0.65	467.75 ± 0.64	468.02 ± 0.64	475.70 ± 0.66

In Table 11 we display information aiming at substantiating the contributions other than $\pi^+\pi^-$ to $a_\mu^{\text{had}}(I = 1)$ – including/excluding the $\gamma \rightarrow \text{hadr.}$ vertex contributions. Integrated over

our energy range of interest, the $\pi^0\gamma$ channel contributes $\simeq 2 \cdot 10^{-11}$, the $\eta\gamma$ channel $\simeq 10^{-11}$, while the $\pi^+\pi^-\pi^0$ and $K\bar{K}$ channels provide contributions at the $\simeq 10^{-12}$ level or less.

The last data column in Table 11 displays the ρ term contribution only, *i.e.* one has canceled out the $\gamma \rightarrow \text{hadr.}$ vertex, and also – for consistency – the FSR contribution; in this case all channels except for $\pi^+\pi^-$ give invisible contributions to the various $a_\mu^{\text{had}}(n)$'s listed. It is also interesting to notice that the main effect of the photon couplings is to reduce the values for the $a_\mu^{\text{had}}(n)$'s.

One should also remind the existence of channels missing the BHLS framework [42] which contribute $(1.34 \pm 0.11) \times 10^{-10}$ to a_μ^{had} . This represents a systematic error clearly of limited influence.

Finally, Table 12 reports on our numerical results for $\mathcal{M}(-n)$ and $\tilde{\mathcal{M}}(-n)$; the first two data columns in the upper part of this Table are a copy out of the central data columns in Table 1 and are reminded for convenience. The third data column shows the effect of only canceling out IB effects – as identified within BHLS. The two rightmost data columns in the lower part of this Table give resp. the moments when keeping the I=1 part of the amplitude *and* the photon terms (direct coupling + FSR) and the last one only when keeping the I=1 component (remind the proviso expressed above). These numbers reflect the same phenomena as commented just above for a_μ^{had} .

6 Conclusion

We have demonstrated that the Mellin-Barnes moments expansion for a_μ^{had} works surprisingly well (see Fig. 2), exhibiting a fast convergence with 4 or 5 moments only. In the timelike approach it assumes the non-perturbative $R(s)$ given for low s and in resonance regions, while the known well-behaved integral kernel $\hat{K}(s)$ of (7) is expanded. Obviously, when $R(s)$ is given the moment expansion is just more elaborate than simply calculating the integral (7) directly. However, in lattice QCD calculations, which are constrained to the Euclidean (spacelike) region, rather than $R(s)$ which is far from being accessible there, the primary object is the electromagnetic current correlator in configuration space

$$\langle J^\mu(\vec{x}, t) J^\nu(\vec{0}, 0) \rangle, \quad (41)$$

where $J^\mu(\vec{x}, t)$ is the electromagnetic current, and various types of moments are extractable from it. Concerning a_μ^{had} the integral representations (1) and (19) reveal that the Euclidean vacuum polarization function $\Pi(Q^2)$ in momentum space is what is needed. So, in principle, a Fourier transform like

$$\Pi(Q^2) (Q^\mu Q^\nu - \delta^{\mu\nu} Q^2) = \int dt e^{\omega t} \int d^3\vec{x} e^{i\vec{q}\vec{x}} \langle J^\mu(\vec{x}, t) J^\nu(\vec{0}, 0) \rangle \quad (42)$$

Table 12: Moments of the a_μ^{had} -expansion in units of 10^{-5} . Here $\mathcal{M}(-n)$ and $\tilde{\mathcal{M}}(-n)$ are evaluated via Eqs. (13) and (14) in terms of $R(s)$ as provided by e^+e^- -annihilation data and/or predictions of the BHLS model Lagrangian. The integration lower limit is $m_{\pi_0}^2$ and the upper limit is $(1.05 \text{ GeV})^2$.

moments HLS scope	Exp. Value		HLS model			
			Standard Fit		γ & I=0 & I=1 (IB removed)	
$\mathcal{M}(0)$	8.6275	± 0.0495	8.6041	± 0.0130	8.1613	± 0.0122
$\mathcal{M}(-1)$	0.22944	± 0.00184	0.23197	± 0.00031	0.22023	± 0.00029
$\mathcal{M}(-2)$	0.008669	± 0.000115	0.008974	± 0.000011	0.008542	± 0.000010
$\mathcal{M}(-3)$	0.0004850	± 0.0000093	0.0005147	± 0.00000064	0.0004902	± 0.0000006
$\mathcal{M}(-4)$	0.00003676	± 0.00000083	0.00003956	± 0.00000005	0.0000376	± 0.000000040
$\tilde{\mathcal{M}}(-1)$	-0.79611	± 0.00501	-0.80054	± 0.00113	-0.75948	± 0.00103
$\tilde{\mathcal{M}}(-2)$	-0.026644	± 0.000294	-0.027334	± 0.000035	-0.026009	± 0.000032
$\tilde{\mathcal{M}}(-3)$	-0.0013149	± 0.0000228	-0.0013847	± 0.0000017	-0.0013193	± 0.0000015
$\tilde{\mathcal{M}}(-4)$	-0.00009063	± 0.00000199	-0.00009725	± 0.00000012	-0.00009253	± 0.00000010

moments HLS scope	Exp. Value		Standard HLS Fit (Breaking effects removed)			
			γ & I=1		I=1 & $\not\gamma$	
$\mathcal{M}(0)$	8.6275	± 0.0495	7.1313	± 0.0096	7.2635	± 0.0100
$\mathcal{M}(-1)$	0.22944	± 0.00184	0.20514	± 0.00027	0.21368	± 0.00030
$\mathcal{M}(-2)$	0.008669	± 0.000115	0.008297	± 0.000010	0.008857	± 0.000012
$\mathcal{M}(-3)$	0.0004850	± 0.0000093	0.0004839	± 0.0000005	0.0005252	± 0.0000008
$\mathcal{M}(-4)$	0.00003676	± 0.00000083	0.00003690	± 0.000000040	0.00004024	± 0.000000058
$\tilde{\mathcal{M}}(-1)$	-0.79611	± 0.00501	-0.69637	± 0.00093	-0.72000	± 0.00100
$\tilde{\mathcal{M}}(-2)$	-0.026644	± 0.000294	-0.025023	± 0.000031	-0.026517	± 0.000036
$\tilde{\mathcal{M}}(-3)$	-0.0013149	± 0.0000228	-0.0013001	± 0.0000015	-0.0014056	± 0.0000020
$\tilde{\mathcal{M}}(-4)$	-0.00009063	± 0.00000199	-0.00009149	± 0.00000010	-0.00009980	± 0.00000014

$Q = (\vec{q}, -i\omega)$ \vec{q} is a spatial momentum and ω the photon energy (input), provides the object required. A Fourier transformation of lattice data, however, is far from being easy and uncertainties due to fluctuations in general turn out to be large (see e.g. in [55]). Moment expansions therefore are often a way out for getting more precise estimates of the HVP function. The Taylor expansion approach (17) with coefficients given by (22) (see also [7, 56, 57]) in conjunction with Padé approximants used in [17], is the simplest one can do. However, the low order Padé approximants we get with 4 moments, illustrated in Fig. 5, are not very convincing for larger momenta in a region which still gives a non-negligible contribution to the a_μ^{had} integral (19).

The Mellin-Barnes moment approach is more promising but also much more elaborate. The reason is that besides the lattice QCD accessible Taylor moments $\mathcal{M}(-n)$ we also need the moments $\tilde{\mathcal{M}}(-n)$. The latter, in the Euclidean regime, require in addition to extract the lattice QCD accessible moments $\Sigma(-n; s_0)$. To our knowledge such an analysis has not yet been performed so far by lattice QCD groups. Our analysis shows that a reliable extraction of the log suppressed $\tilde{\mathcal{M}}(-n)$ is difficult, the main problem being the need for Padé approximants to extend the low energy expansion towards higher energies. Unfortunately, Padé approximants (PA) cannot match QCD asymptotics, which means that one has to use an appropriate cutoff where one can continue the PA with pQCD predictions. In the Euclidean region such a cutoff is expected to be around 2.5 GeV, as one observes by confronting the data extracted Adler function with its pQCD prediction [12, 49]. It means that it is advised to cut the PA of Fig. 5 at 2 GeV to 2.5 GeV in any case and use $\Delta\alpha_{\text{had}}(-Q^2)$ for $Q > Q_1$ or its pQCD prediction. This also has the advantage that one may use the Padé pairs $[n,n]$ and $[n,n+1]$ as upper and lower bounds, keeping integrals convergent.

Note that in order to determine the two sets of moments $\mathcal{M}(-n)$ and the $\tilde{\mathcal{M}}(-n)$, in both cases, in Minkowski space, where we work with data, and in Euclidean space, where we work with Euclidean current correlators, we need and have available only one quantity either $R(s)$ in the first case or $\Pi(Q^2)$ in the second case. The problem on the lattice is that the “trailhead” is always the Euclidean configuration space correlators (41), which allows us to get directly the Taylor moments $\mathcal{M}(-n)$ via (22). However, a corresponding direct configuration space evaluation of the moments $\Sigma(-n; s_0)$, needed to obtain the moments $\tilde{\mathcal{M}}(-n)$, seems not to exist, which means that we have to get $\Pi(Q^2)$ in any case first, by Fourier transformation of the primary configuration space correlators.

Fortunately, it turns out that our master formula (40) for extracting $\tilde{\mathcal{M}}(-n)$ allows for a stable and accurate estimation of the log suppressed moments. This is illustrated in Fig. 9. As an input, an extended (to higher orders) set of Taylor moments $\mathcal{M}(-n)$ is sufficient to allow us to construct the required truncated HVP function to which we have to apply the Padé improvement via $[n-1,n]+[n,n]$ pairs up to some – not too high – cutoff, above which one can include the high energy tail as predicted by pQCD.

Although the moments expansions seem to work surprisingly well, we have some reserva-

tion concerning calculating a_μ^{had} in terms of moments. The moments method emphasizes the low momentum region below the ρ resonance with m_μ as a reference scale. In the standard representations (7) the low energy region also gets enhanced by $1/s^2$, but not more, and we know the ρ resonance yields the dominant piece. It thus properly weights the M_ρ mass region but also has the right high energy behavior to get the integral converge. Our concern is that neither in evaluations based on data nor in lattice QCD estimates (see Figure 5 of [2] and Figure 1 of [14] for recent discussions of that point¹⁸) the low energy tail is easy to get very precisely and therefore the moments expansion tends to increase uncertainties by giving high weight to the problematic region. The problem in lattice QCD of course is that $R(s)$ is not available such that a priori the Euclidean representations (19) or (1) come into play. In the Euclidean region there are no resonances and no flavor thresholds and the structures characterizing the timelike region appear completely smoothed out by the dispersion integrals (28) or (3). So we are confronted with the question where the dominant contributions come from in these representations. The answers are given by Figs. 3 and 1 which show pronounced peaks in the distributions below the 1 GeV scale. To be more precise, the contribution to a_μ^{had} , in the x -integral representations (1) or (19), is the area under the curve shown in the left panels of Figs. 1 and 3, respectively. The figures illustrate the role of extrapolations (especially the large volume limit) still required in order to obtain the bulk of a_μ^{had} . What is used is of course shape information from chiral perturbation theory and from vector meson dominance model type parametrizations which help to control the extrapolation fairly well.

At the end the key problem is how to extract from lattice data of the Euclidean configuration space current correlator (41) a reliable Euclidean HVP function $\Pi(Q^2) = \Pi_{\text{bare}}(Q^2) - \Pi_{\text{bare}}(0)$ or, better, the Adler function $D(Q^2)$, the latter being devoid of problems related to UV subtraction term $\Pi_{\text{bare}}(0)$ and which is bounded in the high energy limit¹⁹. The Taylor + Padé approximants (TPA) method is more sensitive to the high energy tail as becomes obvious from Fig. 5 in conjunction with Fig. 2. The corresponding TPA procedure applied to the Adler function to Q^2 ratio $D(Q^2)/Q^2$, which has a finite limit $Q^2 \rightarrow 0$ and behaves as $1/Q^2$ at higher energies, for the appropriate Padés definitely exhibits a much better behavior in this respect (see Fig. 6) and allows to reduce the uncertainty accordingly.

The Mellin-Barnes moments method is much more elaborate since, besides the Taylor coefficients $\mathcal{M}(-n)$, the log weighted moments $\tilde{\mathcal{M}}(-n)$ are required, which in lattice QCD are much more difficult to evaluate. A major difference between the TPA and the MBM methods seems to be that the MBM method consists in the expansion of the known integral weight func-

¹⁸Present simulations reach typically $Q_{\text{min}} = 2\pi/L$ with $m_\pi L \gtrsim 4$ for $m_\pi \sim 200$ MeV, such that $Q_{\text{min}} \sim 314$ MeV while the kernel displayed in Fig. 1 shows the peak at about 150 MeV.

¹⁹Note that on a lattice in a finite volume $\Pi_{\text{bare}}(0)$ is a difficult object as it is a zero momentum object depending on the lattice spacing and thus requires careful extrapolations $L \rightarrow \infty$ and $a \rightarrow 0$. L the box extension and a the lattice spacing.

tion, not touching the real object of concern, the non-perturbative object $R(s)$. The trick is to focus on $R(s)$ by reweighting it with a series of different magnifying filters. In contrast, the TPA method is based on a low momentum expansion of the non-perturbative object, the Euclidean $\Pi(Q^2)$ or $D(Q^2)/Q^2$ itself.

We think that the use of Padé approximants is not optimal in our context, because the proper QCD high energy behavior cannot be obtained by Padéization of the non-perturbative low energy tail. The upper bounds $[n,n]$ lead to an UV singularity such that only lower bounds $[n-1,n]$ actually can be accepted. To approach the solution one has to consider the convergence of the series $[n-1,n]$ for $n=2,3,4,\dots$. Padé approximants can be very useful to bridge (interpolate) between a low energy and a high energy expansion, as it works very well for the massive 3-loop Adler function (see [12] for details), for example.

We therefore advocate to use the integral representations, preferably (1), directly, as e.g. in [8, 58] and to determine the vacuum polarization function and/or the Adler function as precisely as possible. For both objects $\Pi(Q^2)$ and $D(Q^2)$ rather precise reference functions are available obtained by standard analysis of $R(s)$ data in conjunction with pQCD. Nevertheless, checks with the help of moment expansions are useful to make sure that the obtained vacuum polarization functions are under control. The present analysis provides the “data for the moments” to perform such crosschecks. Needless to say that the moment analysis is much more elaborate than performing the basic integrals once directly. Since the low momentum region is difficult to evaluate in lattice QCD, the minimum momentum on the lattice is $2\pi/L$ where L is the lattice box length. So the access of low momenta is via extrapolation to the infinite volume limit. A promising possibility is the method of analytic continuation proposed in [55], which allows to access low momenta by interpolation, rather than by extrapolation. In this approach one computes the HVP function (42) and varies ω as an input parameter and obtains a smooth function for $\Pi(Q^2 = -\omega^2 + \vec{q}^2)$. Spacelike and timelike momentum regions can be covered and one can reach small momenta and even zero momentum. This is supposed to work under the condition that

$$-Q^2 = \omega^2 - \vec{q}^2 < M_V^2, \quad \text{or } \omega < M_V, \quad (43)$$

where V is the lowest vector state, the lattice realization of the ρ meson in a given simulation.

Unfortunately present computer resources do not yet admit to get precise results in the extended range of interest because simulation data are still too noisy [55], but for the future the method looks very promising.

It should be noted that so far lattice evaluations of the LO a_μ^{had} are mainly based on conserved isovector current calculations and do not include iso-singlet effects (see [59, 60] and references therein, however), isospin breaking effects like $\rho - \omega$ mixing, and electromagnetic

effects like $\rho - \gamma$ mixing [61] or hadronic final state radiation. All these effects are incorporated in our data and in the corresponding BHLS model and fits as described in Sect. 5, if not stated otherwise.

Another question concerns the possible model dependence of the results obtained with the BHLS effective field theory. As the global fit quality of the NSK+KLOE+BESIII data is surprisingly good, it is unlikely that a different or improved model would be able to improve the global fit quality substantially. Actually, different implementations of the Resonance Lagrangian Approach (RLA) are expected to be equivalent provided the high energy behavior is adjusted to be consistent with QCD [62, 63]. Without actually performing a corresponding analysis, e.g. by including additional higher order corrections or by using a different implementation of a RLA model, adding some error would be a plain guess.

In our opinion a model error is already included in our fit errors, since if the model is mismatching with parts of the data of course this is reflected in the global fit error. As an example we mention that dropping photonic corrections from our BHLS model, or not including photonic corrections in any of the alternative RLA implementations, would spoil the good agreement between $\tau \rightarrow \pi^\pm \pi^0 \nu_\tau$ spectral data supplemented by the isospin breaking effects on the one hand and the $e^+ e^- \rightarrow \pi^+ \pi^-$ data on the other hand, as documented by Fig. 11. In other words, neglecting relevant photon-hadron couplings and corresponding loop effects (in self-energies at least), which implies substantial $\gamma - \rho^0$ mixing effects among others, would ruin the excellent BHLS global fit quality. This also implies that photonic corrections have to be included in LQCD calculations at some stage. Taking into account isospin breaking effects originating from the difference in the u and d quark masses, like $\omega - \rho$ mixing, as well as electromagnetic effects, is in progress, but is by far not a simple task.

Acknowledgments

F.J. thanks the Laboratori Nazionale di Frascati (INFN - LNF) for the kind hospitality extended to him. F.J. also thanks Rainer Sommer, Gregorio Herdoíza and Maria Paola Lombardo for helpful discussions.

References

- [1] M. Benayoun et al., arXiv:1407.4021 [hep-ph].
- [2] P. Boyle, L. Del Debbio, E. Kerrane, J. Zanotti, Phys. Rev. D **85** (2012) 074504 [arXiv:1107.1497 [hep-lat]].
- [3] C. Aubin, T. Blum, M. Golterman, S. Peris, Phys. Rev. D **88** (2013) 7, 074505 [arXiv:1307.4701 [hep-lat]].
- [4] G. M. de Divitiis, R. Petronzio, N. Tantalo, Phys. Lett. B **718** (2012) 589 [arXiv:1208.5914 [hep-lat]].
- [5] C. Aubin, T. Blum, M. Golterman, S. Peris, Phys. Rev. D **86** (2012) 054509 [arXiv:1205.3695 [hep-lat]].
- [6] X. Feng, S. Hashimoto, G. Hotzel, K. Jansen, M. Petschlies, D. B. Renner, Phys. Rev. D **88** (2013) 034505 [arXiv:1305.5878 [hep-lat]].
- [7] A. Francis, V. Gülpers, G. Herdoíza, G. von Hippel, H. Horch, B. Jäger, H. Meyer, E. Shintani, H. Wittig, arXiv:1411.3031 [hep-lat].
- [8] M. Della Morte, A. Francis, G. Herdoíza, H. Horch, B. Jäger, A. Jüttner, H. Meyer, H. Wittig, PoS LATTICE **2014** (2014) 162 [arXiv:1411.1206 [hep-lat]].
- [9] R. Malak et al. [Budapest-Marseille-Wuppertal Collaboration], PoS LATTICE **2014** (2015) 161 [arXiv:1502.02172 [hep-lat]].
- [10] G. Bali, G. Endrödi, Phys. Rev. D **92** (2015) 5, 054506 [arXiv:1506.08638 [hep-lat]].
- [11] E. de Rafael, Phys. Lett. B **322** (1994) 239; J. S. Bell, E. de Rafael, Nucl. Phys. B **11** (1969) 611
- [12] S. Eidelman, F. Jegerlehner, A. L. Kataev, O. Veretin, Phys. Lett. B **454** (1999) 369
- [13] <http://www-com.physik.hu-berlin.de/~fjeger/pQCDAdler.tar.gz>
<http://www-com.physik.hu-berlin.de/~fjeger/pQCDAdler.pdf>
- [14] C. Aubin, T. Blum, P. Chau, M. Golterman, S. Peris, C. Tu, Phys. Rev. D **93** (2016) no.5, 054508 doi:10.1103/PhysRevD.93.054508 [arXiv:1512.07555 [hep-lat]].
- [15] A. Francis, B. Jäger, H. B. Meyer, H. Wittig, Phys. Rev. D **88** (2013) 054502 [arXiv:1306.2532 [hep-lat]].

- [16] D. Bernecker, H. B. Meyer, Eur. Phys. J. A **47** (2011) 148 [arXiv:1107.4388 [hep-lat]].
- [17] B. Chakraborty, C. T. H. Davies, P. G. de Oliveira, J. Koponen, G. P. Lepage, arXiv:1601.03071 [hep-lat].
- [18] E. de Rafael, Phys. Lett. B **736** (2014) 522 [arXiv:1406.4671 [hep-lat]].
- [19] R. R. Akhmetshin et al. [CMD-2 Collab.], Phys. Lett. B **578**, 285 (2004)
- [20] V. M. Aulchenko et al. [CMD-2 Collab.], JETP Lett. **82**, 743 (2005) [Pisma Zh. Eksp. Teor. Fiz. **82**, 841 (2005)]; R. R. Akhmetshin et al., JETP Lett. **84**, 413 (2006) [Pisma Zh. Eksp. Teor. Fiz. **84**, 491 (2006)]; Phys. Lett. B **648**, 28 (2007)
- [21] M. N. Achasov et al. [SND Collab.], J. Exp. Theor. Phys. **103**, 380 (2006) [Zh. Eksp. Teor. Fiz. **130**, 437 (2006)]
- [22] A. Aloisio et al. [KLOE Collab.], Phys. Lett. B **606**, 12 (2005);
F. Ambrosino et al. [KLOE Collab.], Phys. Lett. B **670**, 285 (2009)
- [23] F. Ambrosino et al. [KLOE Collab.], Phys. Lett. B **700**, 102 (2011)
- [24] D. Babusci et al. [KLOE Collab.], Phys.Lett. **B720**, 336 (2013)
- [25] B. Aubert et al. [BABAR Collab.], Phys. Rev. Lett. **103**, 231801 (2009); J. P. Lees et al., Phys.Rev. **D86**, 032013 (2012)
- [26] M. Ablikim et al. [BESIII Collab.], arXiv:1507.08188 [hep-ex]
- [27] R. Barate et al. [ALEPH Collab.], Z. Phys. C **76**, 15 (1997); Eur. Phys. J. C **4**, 409 (1998);
S. Schael et al. [ALEPH Collab.], Phys. Rept. **421**, 191 (2005)
- [28] M. Davier et al., Eur.Phys.J. **C74**, 2803 (2014)
- [29] K. Ackerstaff et al. [OPAL Collab.], Eur. Phys. J. C **7**, 571 (1999)
- [30] S. Anderson et al. [CLEO Collab.], Phys. Rev. D **61**, 112002 (2000)
- [31] M. Fujikawa et al. [Belle Collab.], Phys. Rev. D **78**, 072006 (2008)
- [32] R. Akhmetshin et al. [CMD-3 Collab.], Phys.Lett. **B723**, 82 (2013)
- [33] M. Achasov et al. [SND Collab.], Phys.Rev. **D88**, 054013 (2013)
- [34] J. Lees et al. [BABAR Collab.], Phys.Rev. **D87**, 092005 (2013)

- [35] J. Lees et al. [BABAR Collab.], Phys.Rev. **D88**, 032013 (2013)
- [36] J. Lees et al. [BABAR Collab.], Phys.Rev. **D89**, 092002 (2014)
- [37] M. Davier, Nucl. Part. Phys. Proc. **260**, 102 (2015)
- [38] M. Benayoun, EPJ Web Conf. **118** (2016) 01001 doi:10.1051/epjconf/201611801001 arXiv:1511.01329 [hep-ph].
- [39] Z. Zhang, EPJ Web Conf. **118** (2016) 01036 doi:10.1051/epjconf/201611801036 [arXiv:1511.05405 [hep-ph]].
- [40] F. Jegerlehner, EPJ Web Conf. **118** (2016) 01016 doi:10.1051/epjconf/201611801016 [arXiv:1511.04473 [hep-ph]].
- [41] M. Benayoun, P. David, L. DelBuono, F. Jegerlehner, Eur. Phys. J. C **75** (2015) 12, 613 doi:10.1140/epjc/s10052-015-3830-x [arXiv:1507.02943 [hep-ph]].
- [42] M. Benayoun, P. David, L. DelBuono, F. Jegerlehner, Eur. Phys. J. C **73** (2013) 2453 doi:10.1140/epjc/s10052-013-2453-3 [arXiv:1210.7184 [hep-ph]].
- [43] S. Eidelman, F. Jegerlehner, Z. Phys. C **67** (1995) 585 doi:10.1007/BF01553984 [hep-ph/9502298].
- [44] B. E. Lautrup, A. Peterman, E. de Rafael, Phys. Reports 3C (1972) 193
- [45] F. Jegerlehner, Springer Tracts Mod. Phys. **226** (2008) 1. doi:10.1007/978-3-540-72634-0
- [46] <http://www-com.physik.hu-berlin.de/~fjeger/alphaQED.tar.gz>
<http://www-com.physik.hu-berlin.de/~fjeger/alphaQED.pdf>
- [47] W. H. Press, S .A. Teukolsky, W. T. Vetterling, B. P. Flannery, *Numerical Recipes in Fortran* (Cambridge University Press, ISBN 0 521 43064-X, 963 pp).
- [48] F. Jegerlehner, J. Phys. G **29** (2003) 101 [hep-ph/0104304].
- [49] F. Jegerlehner, Nucl. Phys. Proc. Suppl. **181-182** (2008) 135 doi:10.1016/j.nuclphysbps.2008.09.010 [arXiv:0807.4206 [hep-ph]].
- [50] M. Benayoun, P. David, L. DelBuono, F. Jegerlehner, Eur. Phys. J. C **72**, 1848 (2012) doi:10.1140/epjc/s10052-011-1848-2 [arXiv:1106.1315 [hep-ph]].

- [51] K. Hagiwara, R. Liao, A. D. Martin, D. Nomura, T. Teubner, J. Phys. G **38** (2011) 085003 doi:10.1088/0954-3899/38/8/085003 [arXiv:1105.3149 [hep-ph]].
- [52] M. Harada, K. Yamawaki, Phys. Rept. **381**, 1 (2003) doi:10.1016/S0370-1573(03)00139-X [hep-ph/0302103].
- [53] Beringer, J. et al. , "Review of Particle Physics", Phys.Rev. **D86** (2012) 010001.
- [54] T. Fujiwara, T. Kugo, H. Terao, S. Uehara, K. Yamawaki, Prog. Theor. Phys. **73** (1985) 926
- [55] K. Jansen, X. Feng, S. Hashimoto, G. Hotzel, M. Petschlies, D. Renner, PoS LATTICE **2013** (2014) 464.
- [56] K. Maltman, M. Golterman, S. Peris, PoS LATTICE **2014** (2014) 126 [arXiv:1410.7068 [hep-lat]].
- [57] E. B. Gregory, C. McNeile, arXiv:1512.00331 [hep-lat].
- [58] M. Della Morte, G. Herdoiza, H. Horch, B. Jäger, H. Meyer, H. Wittig, arXiv:1602.03976 [hep-lat].
- [59] V. Gülpers, A. Francis, B. Jäger, H. Meyer, G. von Hippel, H. Wittig, PoS LATTICE **2014** (2014) 128 [arXiv:1411.7592 [hep-lat]].
- [60] T. Blum *et al.*, arXiv:1512.09054 [hep-lat].
- [61] F. Jegerlehner, R. Szafron, Eur. Phys. J. C **71** (2011) 1632 doi:10.1140/epjc/s10052-011-1632-3 [arXiv:1101.2872 [hep-ph]].
- [62] G. Ecker, J. Gasser, A. Pich, E. de Rafael, Nucl. Phys. B **321** (1989) 311. doi:10.1016/0550-3213(89)90346-5
- [63] G. Ecker, J. Gasser, H. Leutwyler, A. Pich, E. de Rafael, Phys. Lett. B **223** (1989) 425. doi:10.1016/0370-2693(89)91627-4